Title: Impact of isotype on the mechanism of action of agonist anti-OX40 antibodies in cancer: Implications for therapeutic combinations

Authors: Jane E Willoughby[1], Lang Dou[1,2], Sabyasachi Bhattacharya[3] , Heather Jackson[4], Laura Seestaller Wehr[4], David Kilian[4], Laura Bover[5], Kui S Voo[6], Kerry Cox[1], Tom Murray[1], Mel John[1], Hong Shi[4,] Paul Bojczuk[4], Junping Jing[4], Heather Niederer[7,10], Andrew J Shepherd[8], Laura Hook[7], Steph Hopley[7,11], Tatyana Inzhelevskaya[1], Christine A. Penfold[1], C. Ian Mockridge[1], Vikki English[1], Sara J Brett[4], Roopa Srinivasan[4], Christopher Hopson [4] James Smothers[4], Axel Hoos[4,12], Elaine Paul[13], Stephen L Martin[7], Peter J Morley[9], Niranjan Yanamandra[4†], Mark S Cragg[1†*]

[1]Antibody and Vaccine Group, Centre for Cancer Immunology, School of Cancer Sciences, Faculty of Medicine, University of Southampton, Tremona Road, Southampton SO16 6YD, UK

[2]Current address: TCRcure Biopharma Technology. Building 12, No.6, Nanjiang Second Road, Zhujiang Street, Nansha District, Guangzhou

[3]Current address: IGM Biosciences, 325 E Middlefield Road, Mountain View, CA94043

[4]Immuno-Oncology and Combinations RU, GlaxoSmithKline, 1250 S Collegeville Rd, Collegeville, PA 19426

[5]Immunology Department/ Genomics Medicine Department University of Texas-M.D.Anderson Cancer Center 7455 Fannin St Room 1SCR4.2021; Houston- TX 77054

[6]ORBIT, Institute of applied cancer science; UTMDACC; 7435 Fannin Street; Box 0952 Houston Texas 77030

[7]Biopharm Discovery, GlaxoSmithKline R&D, Gunnels Wood Road, Stevenage, SG1 2NY, UK.

[8]Protein, Cellular and Structural Sciences, GlaxoSmithKline R&D, Gunnels Wood Road, Stevenage, SG1 2NY, UK.

[9]Immunology Research Unit GlaxoSmithKline R&D, Gunnels Wood Road, Stevenage, SG1 2NY, UK.

[10]Current address: Therapeutic Innovation, Cancer Research Horizons, Francis Crick Institute, London, NW1 1AT, UK.

[11]Current address: Apollo Therapeutics, 50-60 Station Rod, Cambridge, CB1 2JH UK

[12]Current address Scorpion therapeutics, 1 Winthrop Square, Suite 400, Boston, MA 02100

[13]GlaxoSmithKline, Research Triangle Park, NC 27709

[†]These authors contributed equally.

*Corresponding authors: Professor Mark Cragg, Antibody and Vaccine Group, MP127, Centre for Cancer Immunology, Cancer Sciences, Faculty of Medicine, University Hospital Southampton, Tremona Road, Southampton, SO16 6YD, UK. msc@soton.ac.uk

Niranjan Yanamandra, Immuno-Oncology and Combinations RU, GlaxoSmithKline, 1250 s, Collegeville Rd, Collegeville, PA 19426. Email: Niranjan.x.yanamandra@gsk.com

Running Title: OX40 mAb therapy

Keywords: OX40, isotype, therapeutic activity

Abbreviations:

ADCC	Antibody dependent cellular cytotoxicity
I.P.	Intraperitoneal
I.V.	Intravenous
KI	Knock-in
KO	Knock-out
mAb	Monoclonal antibody
PBMCs	Peripheral blood mononuclear cells
TILS	Tumor infiltrating lymphocytes
TME	Tumor microenvironment
TNFRSF	Tumor necrosis factor receptor superfamily
WT	Wildtype

Abstract

Background: OX40 has been widely studied as a target for immunotherapy with agonist antibodies taken forward into clinical trials for cancer where they are yet to show substantial efficacy. Here, we investigated potential mechanisms of action of anti-mouse (m) OX40 and anti-human (h) OX40 antibodies, including a clinically relevant monoclonal antibody (mAb) (GSK3174998) and evaluated how isotype can alter those mechanisms with the aim to develop improved antibodies for use in rational combination treatments for cancer.

Methods: anti-mOX40 and anti-hOX40 mAbs were evaluated in a number of *in vivo* models, including an OT-I adoptive transfer immunisation model in hOX40 knock-in (KI) mice and syngeneic tumour models. The impact of FcγR engagement was evaluated in hOX40 KI mice deficient for Fc gamma receptors (FcγR). Additionally, combination studies using anti-mPD-1 were assessed. *In vitro* experiments using peripheral blood mononuclear cells (PBMCs) examining possible anti-hOX40 mAb mechanisms of action were also performed.

Results: Isotype variants of the clinically relevant mAb GSK3174998 showed immunomodulatory effects that differed in mechanism; mIgG1 mediated direct T cell agonism whilst mIgG2a acted indirectly, likely through depletion of Tregs via activating FcγRs. In both the OT-I and EG.7-OVA models, hIgG1 was the most effective human isotype, capable of acting both directly and through Treg depletion. The anti-hOX40 hIgG1 synergized with anti-mPD-1 to improve therapeutic outcomes in the EG.7-OVA model. Finally*, in vitro* assays with hPBMCs, anti-hOX40 hIgG1 also showed the potential for T cell stimulation and Treg depletion.

Conclusions: These findings underline the importance of understanding the role of isotype in the mechanism of action of therapeutic mAbs. As a hIgG1, the anti-hOX40 mAb can elicit multiple mechanisms of action that could aid or hinder therapeutic outcomes, dependent on the microenvironment. This should be considered when

designing potential combinatorial partners and their FcγR requirements to achieve maximal benefit and improvement of patient outcomes.

What is already known on this topic

Several studies have demonstrated efficacy of anti-OX40 monotherapy in murine preclinical models but whilst clinical trials have demonstrated good safety profiles, therapeutic effects have been disappointing.

What this study adds

In this study, we have made use of human OX40 knock-in mice to dissect the impact isotype has on the mechanism of action of anti-human OX40 antibodies; specifically isotype variants of GSK3174998, an anti-human OX40 antibody that has been investigated clinically. We demonstrate that the hIgG1 isotype is the most effective human isotype in our models with the capacity to synergize with anti-mouse-PD-1 and that it can act via both Treg depleting and CD8 activating mechanisms depending on the microenvironment.

How this study might affect research, practice or policy

Our study emphasises the importance of understanding the mechanisms of action of therapeutic antibodies and how that needs to be combined with an understanding of the environment they are acting in, in order to deliver their therapeutic potential. Thus for OX40 to become a viable monotherapy target it may need to be more selectively matched to appropriate tumours. Our study also has implications for how antibody combination therapies are evaluated clinically and the impact of the isotype of each antibody on the availability of FcγR and hence the mechanisms of action of both antibodies.

124

125

Introduction

Antibody immunotherapy now benefits a proportion of cancer patients, most notably after checkpoint blockade in melanoma and non-small cell lung cancer (1, 2). However, with responses only seen in some patients and resistance occurring in others, alternative strategies are being explored (3-5). One option is immune stimulation through tumor necrosis factor receptor superfamily (TNFRSF) members such as OX40 (CD134) (6-10). OX40 is important for T cell proliferation, survival and effector function (11-14), with agonistic antibodies evoking anti-tumor activity in several preclinical models (8, 15-19), leading to the development of a number of clinical candidates. However, monotherapy trials have been disappointing, with limited evidence for efficacy (reviewed in (20)) with checkpoint blockade combinations now being explored (21-26). The addition of anti-PD-1 to anti-OX40 monotherapy is typically beneficial in preclinical models (21, 22, 25), although some studies show anti-PD-1 has a negative impact on anti-OX40 monotherapy (23, 24), leading to considerations of the treatment sequence and the importance of the immune status in each model. One aspect that is under-explored is the impact that isotype can make on monoclonal antibody (mAb) immunotherapy and mechanism of action, particularly in the context of combination therapy.

Anti-mOX40 mAb mechanisms of action are clearly influenced by isotype and interactions with FcγR, with mIgG1 engaging the inhibitory FcγRIIB to trigger OX40 signalling and T cell activation, and mIgG2a depleting OX40+ cells, particularly Tregs (16, 27, 28). Studies have also shown an impact of isotype on anti-PD-1 (29-31). Therefore, as trials look to combine mAb targeting these molecules, an understanding of optimal FcγR interactions for clinically relevant anti-hOX40 mAb is required.

Previously, we reported a hOX40 KI mouse strain, whereby anti-hOX40 mAb with mouse Fc regions demonstrated both antigen-specific CD8+OT-I T cell expansion and anti-tumor responses (16). Here, we extend these studies to examine the humanised clinically-relevant anti-hOX40 hIgG1 antibody GSK3174998, dissect the impact of FcγRs on its mechanisms of action and consider how these may influence potential combinations.

Results

Anti-mOX40 increases effector CD8+ T cells in responsive models.

First, using the anti-mOX40 agonist mAb, OX86 (32), we showed that monotherapy treatment of different tumors delivered variable efficacy (Fig 1A & B and Supplementary Fig 1A-E). There was no impact on tumor growth in LLC and B16 tumors in response to anti-mOX40 treatment whereas EMT6, A20 and CT26 tumors were controlled to varying degrees. To investigate the potential mechanisms involved, tumor infiltrating lymphocytes (TILs) were analysed from mice challenged with CT26 tumors. TILs harvested on day 10 after anti-mOX40 mAb treatment had more CD3+ and CD8+ cells compared with isotype control, alongside more CD8+IFNγ+ and CD8+CXCR5+ cells (Fig. 1C), indicating that they had more effector CD8+ cells (33). Similar results were obtained from A20 tumors; CD8+ T cells isolated from tumors at various time-points showed several immunomodulatory genes were altered by anti-mOX40 mAb treatment (Supplementary Fig. 2A). Furthermore, an increase in CD8+Ki67+ (35.3% vs. 24.3%), CD8+PD-1+ (57.1% vs. 46.8%) and CD8+GzmB+ (34.8% vs. 20.47%) cells was observed (Supplementary Fig 2B), supporting that OX40 treatment leads to an increase in proliferative CD8+ T cells with effector function in the tumor. A significant increase in CD4+Ki67+ (27.7% vs. 20%) and CD8+GzmB+ (6.2% vs. 1.1%) cells was also seen in the blood on day 10 (Supplementary Fig. 2C). Furthermore, PD-1 was upregulated on both CD4 and

CD8+ T cells (8.2% vs. 3.8% and 5.2% vs. 3.3%, respectively) (Supplementary Fig. 2C) indicating anti-mOX40 mAb treatment increases activated CD4 and CD8 T cells with potential for increased functionality both within the tumor and systemically.

To explore other aspects of the T cell response, the TCR repertoire in CT26 tumor-bearing mice was examined after 50 or 100 μg anti-mOX40 mAb. Anti-mOX40 mAb-treated mice showed an increase in TCR clonality in the spleen compared to a pooled group of untreated and isotype controls (Fig. 1D left panel). Untreated and isotype control groups were not significantly different and so pooled to allow more robust statistical evaluation (Supplementary Fig. 2D). Likewise, an increase in TCR clonality was also seen in the tumor (Fig. 1D right panel). Furthermore, the overlap between clones identified in spleen and tumor was increased (Fig.1E). These data indicate that anti-mOX40 mAb drives activation of T cells, promoting clonality and enhancing effector functionality.

Whilst anti-mOX40 mAb monotherapy showed some therapeutic benefit in the models above, the effects were limited. Therefore, combination with checkpoint blockade was investigated. Given the evidence for an upregulation of PD-1 on CD4+ and CD8+ T cells after anti-mOX40 mAb treatment (Supplementary Fig. 2C and (34)), we investigated combination with anti-PD-1 mAb. Treatment of CT26 tumor-bearing mice with anti-mPD-1 mAb monotherapy did not produce significant enhancement of survival (Fig. 1F). Whilst anti-mOX40 mAb monotherapy again showed a modest but significant improvement in survival, the combination with anti-mPD-1 mAb resulted in far greater survival; ~75% of animals survived >50 days compared to ~30% with anti-mOX40 mAb alone (Fig. 1F). The long-term survivors were fully protected from subsequent rechallenge with CT26 (Supplementary Fig. 3A), providing evidence of effective memory generation.

Given the potential impact of dosing schedules on combination therapy (23, 24), we next investigated differences in administration schedules, comparing concurrent or sequential treatments. In the CT26 model, concurrent delivery of anti-mOX40 and anti-mPD-1 mAb resulted in greater efficacy than sequential delivery (Supplementary Fig. 3B) and so subsequent investigations continued with this regimen. To evaluate the impact of the combination on TILs, Nanostring® was performed. The anti-mOX40 and anti-mPD-1 combination increased T cell and immunomodulatory gene transcription in TILs, although the difference from anti-mOX40 monotherapy was subtle (Supplementary Fig. 3C). TIL immune phenotyping showed limited changes in the Tregs (Fig. 1G left panel) but significant increases in the CD8:Treg ratio in mice treated with the combination (Fig. 1G right panel). The CD4+ effector memory (EM) population ($CD62^{low}CD44^{high}$) was increased, with the CD8+ EM population unchanged (Fig. 1H). Further investigation showed that the combination significantly increased the CD8+Ki67+ and CD4+Tbet+ T cell populations in the blood over isotype or anti-PD-1 monotherapy, with a similar trend in the number of CD8+GzmB+ T cells (Supplementary Fig. 3D). However, in TILs the combination treatment resulted in a statistically significant increase in the CD8+GzmB+ population (Supplementary Fig. 3E) but not CD8+Ki67+ or CD4+Tbet+ T cells (Supplementary Fig. 3E), further illustrating the importance of understanding both tumor-localized and systemic responses. Serum levels of effector cytokines IFNγ (Supplementary Fig. 3F), TNFα (Supplementary Fig. 3G), IL-6 (Supplementary Fig. 3H) and IL-2 (Supplementary Fig. 3I) were also significantly increased in the combination arm, to a greater extent than the single treatments. When TCR clonality was examined, only the combination showed an increase in the blood (Fig. 1I left panel) whereas in the tumor, both anti-mOX40 monotherapy and the combination resulted in a significant increase (Fig 1I right panel). The combination did not increase TCR clonality in the tumor above that induced by the anti-mOX40 monotherapy, suggesting that OX40

modulation drives the increase in the tumor. However, the combination increased the number of overlapping expanded clones above that of either monotherapy, supporting the need for both treatment arms (Fig. 1J).

Anti-hOX40 mIgG1 can act directly on antigen-specific T cells.

To help translate these findings, we made use of a clinically relevant humanized anti-hOX40 mAb (GSK3174998) and hOX40 KI mice (16). GSK3174998, was recently explored in a Phase 1/2a trial (ENGAGE-1 - NCT02528357) (26, 35). To explore its potential mechanisms of action in our murine pre-clinical models, it was isotype switched to mIgG1 and mIgG2a isotypes which exhibit differing FcγR binding profiles (36, 37) and effector functions for anti-TNFRSF mAbs (16, 27, 38-41). mIgG2a interacts strongly with activating FcγR and can elicit target cell deletion, whereas mIgG1 binds preferentially to the inhibitory FcγRII, evoking receptor crosslinking leading to agonism and target cell activation.

To explore the impact on antigen-specific CD8 T cell expansion, hOX40KI^{het} OT-I Tg^{het} cells were adoptively transferred into hOX40KI^{hom} recipients before treatment with ovalbumin (OVA) alongside anti-hOX40 mIgG1 or mIgG2a and monitoring for CD8+OT-I+ T cells (Fig. 2A). Anti-hOX40 mIgG1 and mIgG2a expanded CD8+OT-I+ T cells in the blood equivalently during the primary response, although only the mIgG1 group mounted a robust secondary response when challenged with the SIINFEKL ovalbumin peptide (Fig. 2B). These observations, including the mIgG1-dependent memory response, mirror data generated with other antibodies targeting hOX40 (16). Treatment with both isotypes also showed a significant expansion of CD8+OT-I+ T cells in the spleen, albeit to a greater extent with anti-hOX40 mIgG1 (Fig. 2C). CD4+Foxp3+ (Treg) cells expanded in mice treated with the anti-hOX40 mIgG1, but significantly decreased after mIgG2a treatment (Fig. 2D). This

consistently resulted in a fold change of CD4+Foxp3+ T cells >1 with anti-hOX40 mIgG1 and <1 with anti-hOX40 mIgG2a (Fig. 2E).

To explore whether GSK3174998 was acting via different mechanisms dependent upon isotype, purified hOX40KI^{het} OT-I Tg^{het} CD8+ T cells were adoptively transferred into WT C57BL/6 recipient mice, where the anti-hOX40 antibody can act only on the adoptively transferred cells, and the experiment was repeated. The anti-hOX40 mIgG1 again expanded the CD8+OT-I+ T cells (Fig. 2F), supporting a mechanism of direct activation on the CD8+ T cells. In contrast, the mIgG2a variant had no effect, indicating it causes CD8+OT-I+ T cell expansion indirectly, most likely through Treg depletion.

Anti-hOX40mIgG1 requires both activating and inhibitory FcγR for optimal activity. Given this clear isotype-dependent effect, we investigated the role of different FcγR in the CD8+OT-I+ T cell expansion. Accordingly, hOX40KI mice were crossed with either Fcγ chain KO or FcγRIIB KO mice. Fcγ chain KO mice lack expression of all activating FcγR, preventing antibody-mediated target cell deletion (42, 43). In contrast, FcγRIIB loss prevents the receptor crosslinking required for the agonistic activity of anti-TNFRSF antibodies (39-41). Upon adoptive transfer of hOX40KI^{het} OT-I Tg^{het} splenocytes into hOX40KI^{hom} Fcγ chain KO mice, responses to both anti-hOX40 mIgG1 and mIgG2a were reduced (Fig. 3A). The response to anti-hOX40 mIgG2a was almost completely lost as expected if depletion is a key component of this mechanism of action (Fig. 3A right panel). More surprising was the significant reduction in response to anti-hOX40 mIgG1 mAb, presuming receptor crosslinking is important for the activity of this isotype, given FcγRIIB expression is retained and competition from activating FcγR reduced (Fig. 3A left panel). Comparison of the peak responses across multiple experiments confirmed this loss of response with

289 both isotypes of anti-hOX40 mAb, although the anti-hOX40 mIgG1 retained activity
290 significantly above that of the isotype control, unlike the anti-hOX40 mIgG2a,
291 suggestive that the mIgG2a response was disrupted to a greater extent (Fig. 3B). To
292 address whether this was restricted to the blood, spleens were harvested on day 4
293 and T cell populations enumerated. Both anti-hOX40 isotypes, in both strains,
294 showed a significant increase in CD8+OT-I+ T cells (Fig. 3C) although the absolute
295 numbers were lower in the Fcγ chain KO strain. As previously shown, the anti-hOX40
296 mIgG2a mAb decreased the number of Treg in the hOX40KI strain but this reduction
297 was lost in the hOX40KI^{hom} Fcγ chain KO mice (Fig. 3D). These data indicate that the
298 mIgG2a-mediated loss of Tregs in hOX40KI^{hom} mice occurs through depletion
299 mediated via activating FcγR. More surprisingly, the increase in Treg after anti-
300 hOX40 mIgG1 hOX40KI^{hom} was also lost in hOX40KI^{hom} Fcγ chain KO mice (Fig. 3D).
301
302 To investigate the role of FcγRIIB, the experiments were repeated in hOX40KI^{hom}
303 FcγRIIB KO mice. As might be anticipated if FcγRIIB was providing crosslinking for
304 the anti-hOX40mIgG1 mAb, the magnitude of the CD8+OT-I+ T cell response was
305 reduced in the hOX40KI^{hom} FcγRIIB KO recipients (Fig. 3E left panel). In contrast, the
306 response to the anti-hOX40 mIgG2a was unaffected by the loss of the inhibitory
307 receptor (Fig. 3E right panel). Analysis of splenocytes on day 4 also showed less
308 expansion of CD8+OT-I+ cells in the hOX40KI^{hom} FcγRIIB KO recipients treated with
309 anti-hOX40 mIgG1 compared with WT hOX40KI^{hom} recipients whilst the response to
310 anti-hOX40 mIgG2a mAb was significantly above isotype in both strains (Fig. 3F).
311 Analysis of splenic Tregs showed the reduction in numbers mediated via anti-hOX40
312 mIgG2a mAb was maintained in both WT hOX40KI^{hom} and hOX40KI^{hom} FcγRIIB KO
313 strains (Fig. 3G and H), albeit to a lesser extent in the hOX40KI^{hom} FcγRIIB KO strain.
314 The increased number of Tregs and positive fold change seen in response to anti-
315 hOX40 mIgG1, however, was not consistently maintained in hOX40KI^{hom} FcγRIIB KO

mice (Fig 3G and H). The loss of either activating or inhibitory FcγR had a significant impact on the ability of the anti-hOX40 mIgG1 isotype to elicit CD8+OT-I+ T cell expansion, possibly indicating that both are mediating antibody crosslinking.

Anti-hOX40 hIgG1 engages with both activating and inhibitory FcγR to mediate antigen-specific T cell expansion.

We next examined the effect of human isotypes, including the hIgG1 isotype previously used in the clinic. Although this experimental set-up involves interactions between human antibodies and mouse FcγR, the inter-species similarities and differences are known (16, 37) making it possible to interpret the findings and infer likely mechanisms of action for exploitation in patients. Evaluating hIgG1, hIgG2 and hIgG4 variants of the anti-hOX40 mAb, only the hIgG1 was able to robustly expand CD8+OT-I+ T cells in the blood, although the secondary response to SIINFEKL was lower than might be expected (Fig. 4A). Splenic CD8+OT-I+ T cells also showed the greatest expansion in response to anti-hOX40 hIgG1 (Fig. 4B). Only the hIgG1 anti-hOX40 mAb resulted in a statistically significant reduction in the numbers of splenic Tregs (Fig. 4C). To understand whether anti-hOX40 hIgG1 was capable of acting directly on the transferred cells, hOX40KI^{het} OT-I Tg^{het} splenocytes were transferred into WT C57BL/6 recipient mice. As before, only the hIgG1 anti-hOX40 mAb expanded the transferred cells (Supplemental Fig. 4A). To further confirm the direct effect of hIgG1 anti-hOX40 mAb on the antigen-specific CD8+ T cells, purified hOX40KI^{het} CD8+OT-I Tg^{het} cells were transferred into WT recipients and stimulated with OVA and anti-hOX40 mAb. Again, only anti-hOX40 hIgG1 expanded the CD8+OT-I+ cells (Fig. 4D).

Given these observations, we focused on the importance of the different FcγR. hIgG1 interacts with multiple activating mouse and human FcγR and so we hypothesised

that these interactions were responsible for the observed reduction in splenic Tregs. To test this, hOX40KI^{het} OT-I Tg^{het} cells were transferred into hOX40KI^{hom} or hOX40KI^{hom} Fcγ chain KO mice prior to OVA and anti-hOX40 mAb stimulation. In the hOX40KI^{hom} Fcγ chain KO strain the expansion of CD8+OT-I+ T cells was significantly lower than in the hOX40KI^{hom} strain and insufficient to elicit a secondary response to SIINFEKL peptide (Fig. 4E). Analysis of splenocytes on day 4 showed reduced expansion of CD8+OT-I+ T cells in the hOX40KI^{hom} Fcγ chain KO strain (Fig. 4F). No consistent Treg depletion was observed in the hOX40KI^{hom} Fcγ chain KO mice (Fig. 4G; Supplemental Fig. 4B), resulting in a significant difference between the Treg fold change induced by anti-hOX40 hIgG1 in hOX40KI^{hom} versus hOX40KI^{hom} Fcγ chain KO recipients. As there was still some expansion of CD8+OT-I+ T cells in the hOX40KI^{hom} Fcγ chain KO mice above the isotype control, the role of FcγRIIB was explored in hOX40KI^{hom} FcγRIIB KO mice. Despite variation between experiments, pooled data showed a slight reduction in expansion of CD8+OT-I+ cells in hOX40KI^{hom} FcγRIIB KO compared WT hOX40KI^{hom} mice (Fig. 4H and Supplemental Fig. 4C). Likewise, as the response contracted into memory phase (day 40), significantly greater percentages of CD8+OT-I+ T cells were observed in the hOX40KI^{hom} strain than the hOX40KI^{hom} FcγRIIB KO mice (Fig. 4I) suggesting that FcγRIIB has a role in the generation or persistence of memory. This translated into a greater secondary response in hOX40KI^{hom} versus hOX40KI^{hom} FcγRIIB KO mice (Supplementary Fig. 4D). Similarly, in the spleen at day 4, CD8+OT-I+ T cells significant increased in both strains (Fig. 4J). These data indicate that there is an initial expansion of CD8+OT-I+ T cells in the hOX40KI^{hom} FcγRIIB KO mice but that the response is not maintained, which leads to a lower overall recall response. Analysis of splenic Tregs in the hOX40KI^{hom} FcγRIIB KO strain was inconclusive when analysed as individual experiments (Fig. 4K); however, when analysed across multiple experiments, a fold change <1 (Fig. 4L) was seen, suggesting FcγRIIB is not

important for Treg depletion. Thus, these data suggest that anti-hOX40 hIgG1 mAb mediates its effects through depletion of Tregs via the activating FcγR as well as by acting directly on the CD8+ T cells with cross-linking provided by FcγRIIB.

Anti-hOX40 hIgG1 combination with anti-mPD-1 improves efficacy in EG7-OVA model.

Next, we explored the therapeutic efficacy of the various anti-hOX40 mAb in a murine tumor model. Mice were challenged with E.G7-OVA thymoma cells and then treated once tumors had developed as outlined in Fig. 5A. Anti-hOX40 mIgG2a caused a slight delay in tumor growth (Fig. 5B) which resulted in 15% long-term survivors (>50 days) across 3 independent experiments (Fig. 5C). The anti-hOX40 mIgG1 resulted in a significant reduction in tumor growth (Fig. 5B) with 47% long-term survivors (Fig. 5C). For both isotypes, long-term survivors were protected from rechallenge with E.G7-OVA (Supplemental Fig. 5A and B). These data show that for this particular antibody, mIgG1 provides greater efficacy than mIgG2a and infer that depletion of Tregs may be less beneficial than direct CD8 activation. Given that anti-hOX40 hIgG1 had shown potential to mediate both depletion and direct activation we investigated its efficacy in the E.G7-OVA model versus hIgG2 and hIgG4. Although mean changes in tumor growth were not significantly different (Fig. 5D), anti-hOX40 hIgG1 gave more long-term survivors (28%) compared to hIgG2 (10%) or hIgG4 (0%) (Fig. 5E), with long-term survivors showing resistance to rechallenge with E.G7-OVA (Supplemental Fig. 5C). As the efficacy of the anti-hOX40 hIgG1 mAb in this model was relatively limited, and following our earlier results with anti-mOX40 mAb, combination with anti-mPD-1 mAb was assessed. As anti-mPD-1 efficacy is reduced when there is insufficient priming of CD8 T cells (44), a staggered dosing schedule, employing anti-hOX40 hIgG1 mAb first, as outlined in Fig 5F, was used. Mice treated with anti-mPD-1 monotherapy showed no reduction in tumor growth, whilst

those treated with anti-OX40 hIgG1 and the combination showed tumor control (Fig. 5G). Anti-mPD-1 monotherapy showed a marginal improvement in survival but with no long-term survivors whereas anti-hOX40 hIgG1 resulted in a significant improvement in survival with 21% long-term survivors (Fig. 5H), which was enhanced in the combination; 46% of mice surviving >90 days (Fig. 5H). In a following experiment where a staggered and concurrent dosing strategy were compared, we did not observe a significant difference in the strategies, suggesting that concurrent dosing is also effective in this model (Supplementary Fig. 5D-F). These data support combining anti-hOX40 and anti-mPD-1 mAb in the clinic to achieve improved tumor control compared with monotherapy.

Anti-hOX40hIgG1 can elicit cytokine secretion from hPBMCs and preferentially targets hTregs in ADCC reporter assays

To see if the combination of anti-hOX40 hIgG1 and anti-PD-1 could trigger higher T cell activity in humans, PBMCs from healthy donors were activated with anti-CD3 and anti-CD28 in the presence of anti-hOX40 hIgG1 and pembrolizumab and then analysed for IFNγ (Supplemental Fig. 6A) and TNFα (Supplemental Fig. 6B) secretion. For both cytokines, the combination resulted in the highest secretion, suggesting that in patients, this combination may also result in a greater immune response.

To consider which patient groups might benefit most from treatment with anti-hOX40 mAb, we analysed the TCGA database for expression of OX40, OX40L and PD-L1. The expression of all three markers varied widely across tumor types (Supplemental Fig. 6C) however renal cell carcinoma (RCC) and sarcoma samples showed high levels, particularly of OX40 and so may be good options for combination therapy. To explore this further, we performed flow cytometric analysis of patient tumor samples. The majority of CD3+ TILS within resected tumor samples (NSCLC, CRC, Bladder,

Head and Neck, Thyroid, Prostate, Cervical, Endometrial, Gastric and RCC) were CD4+, with lower numbers of CD8+ T cells and a minority of Treg (Fig. 6A). However, OX40 on these T cell subsets was inversely correlated with their cellular frequency, with both percent OX40 positivity and number of molecules/cells being highest on Treg > CD4+ > CD8+ T cells, as indicated previously (45-47) (Fig. 6B and C). These data suggest that anti-hOX40 mAb might preferentially target Tregs and CD4+ effectors over CD8+ T cells. This hierarchy was also observed when PBMCs, isolated from healthy donors or cancer patients, were activated for 2 days, with Tregs showing the greatest number of OX40 receptors/cell, followed by CD4+ effectors and CD8+ T cells (Fig. 6D). Given that in the hOX40KI mouse model, the anti-hOX40 hIgG1 mAb depleted Tregs in the presence of activating FcγR, an in vitro ADCC reporter assay was performed to evaluate the ability of different T cell subsets to engage hFcγRIIIA (as a readout for depleting potential) once opsonised with mAb. To better mimic ongoing immune response in the tumor, healthy donor or patient PBMCs were activated in vitro with anti-CD3/anti-CD28, sorted into the respective cell populations, and then incubated with anti-hOX40 hIgG1 mAb and hFcγRIIIA-expressing reporter cells. Treg showed the greatest ability to engage hFcγRIIIA and induce luciferase expression (Fig. 6E), with the number of OX40 receptors strongly correlated with luciferase induction across all cell types (Fig. 6F). This relationship between the number of OX40 receptors and the ability to engage hFcγRIIIA, suggests a potential mechanism of action in patients with Tregs the primary target for depletion.

Discussion

In agreement with previous reports, we showed that anti-mOX40 monotherapy could be efficacious in several mouse tumor models. When mouse IgG isotypes were examined, our results were consistent with those targeting other TNFRSF members

(16, 39, 48), namely that mIgG1 was agonistic, acting directly on CD8+OT-I+ T cells whilst mIgG2a acted indirectly, most likely through depletion of Tregs. FcγR KO mice studies supported this hypothesis, with anti-OX40 mIgG2a activity and Treg depletion requiring the presence of the γ chain (activating FcγR), whilst loss of the FcγRIIB had no impact. In contrast, for anti-OX40 mIgG1 loss of both inhibitory and activating FcγR had an impact. The loss of the crosslinking activity of the FcγRIIB was predicted to impact the CD8+OT-I+ T cell expansion (39-41), however the reduction in the expansion in the γ chain KO strain was unexpected. Whilst activating FcγR are typically considered to recruit effector immune cells with a depleting capacity, it is possible they could also provide crosslinking. The principal ability of all FcγR to evoke mAb:receptor cross-linking has been shown previously, with the reliance on FcγRIIB thought to reflect amenable expression patterns and location (49, 50). The mIgG1 primarily interacts with mFcγRIIB and mFcγRIII, both of which are low affinity receptors (51, 52) and so it is possible that on cells that lack the high affinity FcγRI, such as NK cells and neutrophils, these low affinity receptors combine to provide crosslinking. In the γ chain KO mice the mFcγRIII component is lost, resulting in crosslinking from only FcγRIIB and hence a potential reduction in expansion. These data are surprising given that the same observation was not made for CD40 (41) or 4-1BB in tumor models (39) but this may be reflective of OX40's requirement for higher order oligomerisation for signalling whilst CD40, at least, has been suggested to pre-exist in low order oligomerisation (28, 53) and so may require lower levels of crosslinking. Alternatively, it may reflect that activating FcγR deliver additional signals into important immune cells (such as DC), serving to boost immune responses, as proposed previously (54, 55).

Expanding this analysis into the E.G7-OVA tumor model, we showed that for GSK3174998 antibodies, a mIgG1 isotype provides greater efficacy than mIgG2a. Whilst this may suggest that direct CD8 activation would be the more effective

mechanism in this model, previous studies with a panel of antibodies against hOX40 had not shown this isotype preference (16), indicating a potential epitope dependence.

To explore more clinically relevant settings, hIgG isotypes of GSK3174998 and their potential mechanisms of action were also explored. The hIgG1 variant resulted in the greatest expansion of CD8+OT-I+ T cells > hIgG2 and hIgG4, whilst also causing Treg loss. Further studies showed that as with the mIgG1, the hIgG1 variant was capable of acting directly on CD8+OT-I+ T cells, albeit more modestly than the mIgG1, suggesting that hIgG1 can act via both direct agonism and depletion of Tregs. Experiments in the FcγR KO mice supported this hypothesis as both the loss of the activating FcγR (γ chain KO) and FcγRIIB impacted the ability of the hIgG1 to expand CD8+OT-I+ T cells. Extending this analysis to the E.G7 tumor model, the hIgG1 isotype (GSK3174998) was again more effective than hIgG2 and hIgG4. Whilst the hIgG1 showed similar attributes to both the mIgG1 (in terms of efficacy and mechanism) and mIgG2a (Treg depletion) it is important to note that in terms of FcγR engagement, structure and FcγR independent functions there are no direct homologues between mouse and human IgG (51) and hence it can deliver both deletion an agonism unlike the mouse isotypes. Perhaps slightly more surprising is the lack of efficacy with the hIgG2. hIgG2 antibodies have been shown capable of evoking powerful target receptor agonism in an FcγR independent manner (reviewed in (56)) when targeting various TNFR, due to the unique hinge of hIgG2 (57). However, this effect is not seen in all antibodies; for example, the anti-4-1BB mAb Urelumab but not Utomilumab is rendered more agonistic as a hIgG2 than a hIgG1 (58). Thus, it suggests that GSK3174998 may be more in line with Utomilumab in that isotype switching to hIgG2 does not render it more agonistic and hence delivers a less impressive impact both in OT-I expansion and efficacy in the E.G7 tumour

model than anticipated. Another interesting point is that despite showing properties similar to the mIgG1, the hIgG1 never performed as well as the mIgG1 in the E.G7 model (28% vs 47% long-term survivors, respectively). One possible explanation is the use of a human isotype engaging mouse FcγR; however, human isotypes, including hIgG1, have been shown to interact with mouse FcγR effectively to elicit cell depletion (52). Another possibility is that the capacity for engaging both activating and inhibitory FcγR results in competition for effector mechanisms which is detrimental to overall efficacy. As our knowledge of the interaction between hIgG and FcγR continues to increase, new mutations are being introduced into hIgG with the aim of increasing or decreasing affinity for different FcγR. Campos Carrascosa et al. recently showed that an engineered anti-OX40 hIgG1-V12 mAb with increased binding to hFcγRIIB resulted in increased TIL proliferation compared with the WT hIgG1 antibody (28). Whilst this approach looks promising, the availability of FcγR in the tumor microenvironment in different cancers will presumably prove crucial in determining whether increasing affinity for the inhibitory receptor is a fruitful line of development. Indeed, whilst our data suggests that the hIgG1 isotype should be the preferred isotype to take to the clinic, anti-OX40 hIgG1 mAb have shown limited efficacy in the clinic to date (26, 59-61). There are several potential explanations for this lack of translation from preclinical models including 1) the relatively lower cytotoxicity potential of hIgG1 vs mIgG2a; 2) the higher affinity of hIgG1 for the human inhibitory receptor; 3) the upregulation of FcγRIIB in human tumours (62) and 4) the relative paucity of Treg in human cancers versus murine models. Therefore, it maybe that OX40 hIgG1 would only be capable of having clinical impact in tumours where Treg were 1) prevalent, 2) the main mechanism limiting immune response and 3) capable of deletion due to a permissive FcγR expression pattern. It has already been questioned whether Treg prevalence in many human tumours is sufficient to act as an effective immunomodulatory target (63) and whether anti-CTLA-4 mAb operate

through Treg deletion in humans (64) despite abundant and clear evidence in mouse models (including with human FcγR expressing mice) (45, 65). To evaluate this and deliver clinical benefit, it may be necessary to biopsy for sufficient Treg presence and amenable FcγR expression patterns in patients and optimise the OX40 mAb Fc for higher A:I ratio, through targeted mutations and/or glycoengineering (66).

In considering these aspects, a limitation of our study is that the pre-clinical mouse models do not fully recapitulate the human FcγR expression profile seen in human tumours. A further limitation of our study is that is that it utilises a chimeric human:mouse OX40 model. Whilst we have previously shown that the hOX40KI model does broadly mimic expression patterns of human OX40 (16), it more closely reflects the expression pattern of mouse OX40 and moreover, does not contain the human signalling domain and machinery, leading to potential differences to those observed in the clinic.

As introduced above, one of the strategies being explored in the clinic is the combination of anti-OX40 with anti-PD-1. In line with other pre-clinical studies combining PD-1/PD-L1 axis blockade with anti-OX40 mAb (22, 34), we were able to show improved therapy in both the CT26 and E.G7-OVA models (Fig 2F, 5G and H). Furthermore, this combination increased IFNγ and TNFα production from healthy human donor cells (Supp Fig 6 A and B). Despite this, and a body of supportive pre-clinical data, results from clinical trials indicate this combination will not be transformative in patients (21, 26). One possibility is that further understanding of dosage/scheduling is needed for the pre-clinical efficacy to be translated into the clinic. Different pre-clinical models have shown conflicting data as to whether concurrent treatment with anti-PD-1 and anti-OX40 is beneficial or detrimental (22-24, 34). Wang et al. investigated this based on responses to BMS-986178 in patients and comparison with their surrogate antibody OX40.23 in the CT26 model and showed that OX40 expression was lost following high receptor occupancy (25).

Through modelling, they suggested that there may be a need for adjusting dosing and scheduling to achieve lower occupancy than is desired traditionally when using receptor-blocking entities such as checkpoint inhibitors.

Another consideration, especially when developing combinations of antibodies is the competition for FcγR. Here, we showed that anti-OX40 requires multiple FcγR for its maximal immune stimulating properties (both in vivo and in vitro using hPBMCs), and whilst we did not directly investigate the FcγR requirement for the anti-PD-1, others have previously shown that FcγR engagement impacts the efficacy of anti-PD-1 mAb (29-31). Therefore, there is a possibility that competition for FcγR between the two mAbs could limit the combinatorial impact. Anti-PD-1 mAbs in the clinic are mostly hIgG4, selected for reduced capacity for FcγR engagement, however they retain appreciable affinity for FcγRI (51, 52), which likely limits their efficacy. Indeed Moreno-Vicente et al recently compared anti-PD-1 hIgG4 and anti-PD-1 hIgG4 FALA (Fc null) mAbs in mice expressing hFcγR, showing the Fc null variant gave enhanced effects (30). Although the immune context during immunisation clearly differs from that in a tumor model, or cancer patient, this aspect of competition for FcγR engagement should be more widely explored.

Whilst our data agrees with the concept that targeting OX40 and particularly the combination with checkpoint blockade could be a therapeutic option, clearly more is still needed for this to be translated successfully to the clinic. A greater understanding of what is needed for OX40 therapies to work in pre-clinical models and the difference between those models where treatment fails or succeeds, may provide the insight to deliver favourable outcome in patients. Similarly, lessons from the clinic in terms of FcγR profiles, cellular compositions and spatial arrangements in conjunction

with biomarkers for underpinning immune mechanisms, in relation to varying dose, will help inform how to develop more effective strategies targeting OX40 in the future.

Material and Methods

Primary human samples

hPBMCs were obtained from whole blood following centrifugation through a density gradient medium. Surgically resected cancer patient tumor tissues were obtained from Avaden Biosciences (Seattle), shipped overnight. Fresh tumors were dissociated immediately upon arrival, and within 24 hours of surgical resection using GentleMacs Human Tumor Dissociation kit (Miltenyi Cat. #130-095-929). Baseline immune phenotyping occurred immediately upon tumor dissociation.

Mice

C57BL/6, BALB/C and OT-I mice were obtained from Charles River Laboratories or Envigo. hOX40KI were generated by Ozgene (16). hOX40KI/OT-I mice were generated in house. Young adult mice were sex- and age-matched and randomly assigned to experimental groups. Experiments were not blinded.

Antibody Production

Anti-hOX40 mAb was produced as previously described (13). Isotype switching was performed by cloning V regions into mammalian expression vectors encoding mIgG1, mIgG2a, hIgG1, hIgG2 or hIgG4 (S228P L235E to minimise hIgG4 Fab arm exchange) constant regions. Antibodies were expressed by transient transfection of HEK293 cells and purified from supernatants by protein A affinity chromatography using MabSelect SuRE columns (GE Healthcare) followed by size exclusion chromatography (SEC) using Superdex 26/60 200 SEC columns (GE Healthcare). All preparations were filter sterilised (0.2 µM) and endotoxin low (<2 EU/mg protein).

615 ADCC reporter assays

616 PBMCs from healthy human donors were cultured for 42 hours ± human T activator
617 CD3/CD28 Dynabeads (Gibco). CD4+ T effector and Treg cells were isolated with
618 the EasySep Human CD4+CD127lowCD25+ Regulatory T cell Isolation kit (Stemcell)
619 and CD8 T cells with Dynabeads CD8 Positive Isolation Kit (Invitrogen). These cells
620 were treated with anti-hOX40 antibodies or isotype controls and used as targets in
621 the ADCC Reporter Bioassay kit (Promega) at a 1:6 ratio, incubated at 37^{o}C for 6
622 hours. Luminescence was read using an Envision plate reader.

623

624 OX40 Receptor density determination

625 Quantification of OX40 levels was assessed using PE-labelled GSK3174998 with BD
626 QuantiBrite beads (BD Biosciences) via flow cytometry. Spearman correlation
627 coefficients and two tailed t-tests were calculated in GraphPad Prism using the total
628 OX40 receptor values and the fold induction obtained for each cell type.

629

630 Flow cytometry

631 Flow cytometry antibodies are listed in Table 1. Intracellular staining was performed
632 using Foxp3 staining buffer kit (ThermoFisher-eBioscience) or Transcription Factor
633 Buffer set (BD Biosciences) according to the manufacturer's protocol. All flow
634 cytometry experiments were performed on either a FACSCanto II or Fortessa (BD
635 Bioscience). Data analysed using FACSDiva (BD Bioscience) or FlowJo (BD
636 Bioscience).

637

638

639

640

641

642

Target	Clone	Company
mCD8a	53-6.7	ThermoFisher-eBioscience
mCD4	GK1.5	ThermoFisher-eBioscience
mCD3	145-2C11	ThermoFisher-eBioscience
mFoxp3	FJK-16s	ThermoFisher-eBioscience
mCD62L	MEL-14	ThermoFisher-eBioscience
mCD44	IM7	ThermoFisher-eBioscience
H-2K^{b}/SIINFEKL tetramer		Southampton University
isotypes		Corresponding companies
hCD4	RPA-T4	BD-Biosciences
hCD8	RPA-T8	BioLegend
hFoxP3	PCH101	eBioscience
hCD25	BC96	BioLegend
hOX40	ACT-35	eBioscience

643 Table 1. – Flow cytometry antibodies used.

644

645 OT-I Adoptive Transfer

646 1x10^{5} hOX40 KI$^{+/-}$ OT-I cells were injected i.v. into hOX40 KI$^{+/+}$ or WT C57BL/6 mice.
647 24 hours later 5mg ovalbumin (Sigma) and 100μg anti-hOX40 or isotype control were
648 given i.p. Splenic analysis was performed by harvesting spleens day 4 post i.p. OT-I
649 kinetics were monitored in the blood through SIINFEKL tetramer staining and mice
650 were rechallenged 6-10 weeks later with 30 nM SIINFEKL (PeptideSynthetics) i.v.
651 once the memory T cell population had contracted to less than 1% of the single cell
652 population. Mice with SIINFEKL tetramer responses <1% of CD8+ lymphocytes at
653 the peak of the response were excluded due to the likelihood that OT-I transfer had
654 failed since isotype controls peak at an average 5.2% +/- 0.58 s.e.m. (mIgG1) and
655 4.65% +/- 0.65 s.e.m. (mIgG2a) in blood and 3.8% +/- 0.79 s.e.m (mIgG1) and 3.1%
656 +/- 0.89 on day 4 in spleens. Exclusions based on these criteria are indicated in
657 Figure Legends.

658

659 Tumor Models

660 CT26: 5x10^{4} CT26 (ATCC: CRL-2638) mouse colon carcinoma cells were inoculated
661 subcutaneously into the flank of BALB/C mice. Palpable tumors were measured
662 using callipers with tumor volume calculated using (L x W x H)/2 or 0.52 x Length x

Width^2. Mice (n = 7–13/treatment group) were randomized when tumors reached approximately 100–150 mm^3 and treated with anti-mOX40 rat (r)IgG1 (clone OX86, BioXCell BE0031), anti-mPD-1 rIgG2a (clone RPM1-14, BioXCell BE0146) or their respective isotype controls, rIgG1 (clone HRPN, BioXCell BE0088) or rIgG2a (clone 2A3, BioXCell BE0089). Antibodies were given i.p. twice/week starting on randomization day for a total of 6 doses for efficacy studies or up to 3 doses for pharmacodynamic studies. In combination experiments with CT26, antibodies were dosed concurrently. Mice were removed from the study when maximal tumour size was reached (either 2,000 or 4000 mm^3, depending on study site). Mice were also removed due to weight loss (> 20%), ulceration or tumor necrosis, or any obvious inhibition of normal mouse activity.

E.G7-OVA: 5x10^5 E.G7-OVA cells were injected subcutaneously into the flank of hOX40KI$^{+/+}$ mice. Based on preliminary experiments n = 5 was determined as sufficient to see a $p < 0.05$ for tumor therapy. Groups of 8 mice were inoculated to ensure a minimum of 5/group with established tumors with comparable size (between 5x5 and 8x8 mm) for treatment. Mice were then ranked according to tumor size and assigned to treatments groups so that average tumor size per group was equivalent. This ensured mixed treatment groups within cages to reduce the influence of housing on treatment effect. Mice received 3 x 100 µg anti-hOX40 mAb or isotype i.p. every 3rd day. Mice were culled once they reached humane endpoint (20 x 20 mm) or end of experiment if long-term survivors. Mice which eradicated tumor after treatment were rechallenged with 5x10^5 E.G7-OVA s.c. into the flank. Combination experiments of anti-OX40 hIgG1 (100 μg) and anti-PD-1 rIgG2a (250 μg; clone RPM1-14, BioXCell BE0146) were performed as outlined in Fig 5F.

Pharmacodynamic studies

Mouse pharmacodynamic studies were performed in A20 or CT26 mouse models following monotherapy or combination treatment. In monotherapy studies, animals were dosed with 100μg rIgG1 or anti-mOX40 rIgG1 (OX86) once or twice a week and harvested 48 hours following the third dose. In combination studies, mice were randomized into five groups receiving vehicle, isotype control (rIgG1 100 μg + rIgG2a 200 μg), anti-mOX40 (OX86 100 μg +rIgG2a 200 μg), anti-PD-1 (PD-1 200 μg + rIgG1 100 μg) or anti-mOX40 and anti-PD-1 (OX86 100 μg +PD-1 200 μg). Mice were dosed twice a week on day 0, 3 and 7 and blood and tumor harvested on day 3, 7 and 10 following the first dose equating to 1, 2 and 3 doses, respectively. Tumor samples collected were subjected to dissociation using Miltenyi Tumor Dissociation Kit cocktail (Miltenyi Biotec, Cat#130-096-730) for 40 minutes at 37°C. After digestion, and filtration, $1x10^5$ cells were pre-blocked where necessary with human or mouse Fc block (Miltenyi Biotec) and stained with detection antibodies.

Statistics

All results show mean ± standard error of the mean (SEM). One way Annova with multiple comparisons (Dunnett's, Tukey's or Sidak's as stated in legend) or Mann Whitney tests were used as stated in legends, performed using GraphPad Prism. Survival curves were evaluated using a Log-rank (Mantel-Cox) test. Significance shown relative to isotype control unless bar is shown. Where indicated ns = not significant, * $p \leq 0.05$, ** $p \leq 0.01$, *** $p \leq 0.001$, **** $p \leq 0.0001$.

Declarations

Ethics Approval

All studies were conducted in accordance with the GSK Policy on the Care, Welfare and Treatment of Laboratory Animals and were reviewed by the Institutional Animal Care and Use Committee either at GSK or by the ethical review process at the

institution where the work was performed. Studies performed at the University of Southampton were conducted in accordance with UK Home Office guidelines, under PPL P4D9C89EA and were additionally approved by the University of Southampton's AWERB committee.

Human biological samples were sourced ethically and used in accordance with informed consent. Patient material was obtained with the appropriate informed consent in accordance with the GSK human biological sample management policy and standard operating procedure. Healthy blood for PBMC obtained from GSK: Quorum (Advarra) Protocol #24109QMR/3. Tumour samples for the TILs were brought from Avaden Bio.

Availability of Data and Material

All datasets used and/or analysed during the current study are available from the corresponding author on reasonable request.

Acknowledgements

We are grateful to the staff of the University of Southampton Biomedical Research facility for their technical support. We also thank Leon Douglas and Patrick Duriez from the ECMC/CRUK funded Protein Core Facility for making SIINFEKL tetramers

Author contributions

JW, LD, KC, TM, SB, HJ, DK, HS, PB, J, LB, KV and LSW performed experiments. JW, LD, SB, HJ, DK, HS, PB, J, LB, KV and LSW performed statistical analyses. MJ, VE, TI, CP, HN, AS, SH, and LH provided technical support, reagent generation and QC. JW, LD, SB, HJ, DK, HS, PB, J, LSW, PM, SB, NY and MSC designed experiments. JW, RS, JS, AH, EP, SM, SB, PM, NY and MSC provided concept

leadership. JW, PM, NY and MSC wrote the manuscript. All authors contributed to manuscript revision and read and approved the submitted version.

Funding

This study was funded by GSK.

Conflict of interest

MSC is a retained consultant for BioInvent International and has performed educational and advisory roles for Baxalta and Boehringer Ingleheim. He has consulted for GSK, Radiant, iTeos Therapeutics, Surrozen, Hanall and Mestag and received research funding from BioInvent, Surrozen, GSK, UCB and iTeos. SB, HJ, LSW, DK, HS, PB, JJ, HN, AS, LH, SH, SB, RS, JS, AH, EP, SM, PM and NY are (or were at the time the work was conducted) employees of GSK.

Figure Legends

Figure 1. anti-mOX40 rIgG1 mAb results in an activated immune response in CT26 syngeneic tumor models. A. Schematic of mice challenged with $5x10^5$ CT26 tumor cells and subsequent treatment with either isotype control or anti-mOX40 (OX86) mAb (100 μg) twice weekly. B. Growth curves of mice challenged with CT26 cells and treated as depicted in A; n = 10 (similar trends observed in multiple studies). C. Mice inoculated with $5x10^5$ CT26 tumor cells were harvested 10 days post initial treatment with TILs assessed by flow cytometry for CD45+CD3+ (left panel), CD8+ (left middle panel), CD8+IFNγ+ (right middle panel) and CD8+CXCR5+ (right panel). N = 7 isotype control and n = 5 for anti-mOX40, one experiment. D. Mice inoculated with $5x10^5$ CT26 tumor cells 7 days post treatment with indicated doses of anti-OX40. Spleens (left panel) and tumor (right panel) were harvested and assessed for TCR repertoire clonality; n = 3 except the combined group of isotype and untreated

where n=6, one experiment. E. Analysis of the overlap of TCR CDR3 clones between spleen and tumor analysed in D; n = 3 except the combined group of isotype and untreated where n = 6, one experiment. F. Survival curves of mice challenged with $5x10^5$ CT26 SC and treated with either anti-mOX40 (100 μg), anti PD-1 (200 μg) or combination of anti-mOX40 and anti-PD-1 dosed as outlined in A. n = 10 for isotype, anti-mOX40 and anti-PD-1, n = 20 for anti-mOX40 + anti-PD-1. Similar trends were observed in multiple studies. G-H TILs harvested on Day 10 and immunophenotyped for Treg (G – left panel), CD8:Treg ratio (G right panel) and effector memory cells (CD62L low CD44 high) (H). n = 5, one experiment. I. TCR repertoire clonality analysis for blood (left panel) and tumor (right panel) from CT26-bearing mice harvested on Day 15; n = 7, except for tumor sample treated with anti-PD-1 where n = 6, one experiment. J. Analysis of the overlap of TCR CDR3 clones between blood and tumor. N = 7, one experiment **** $p < 0.0001$, *** $p < 0.001$, ** $p < 001$, * $p < 0.05$ Mean +/- SEM B. Sidak's multiple comparison one-way ANOVA, C & E – unpaired T-Test, D-E - Dunnet's multiple comparison one-way ANOVA, F- Log-rank test, G-J – Tukey's multiple comparison one-way ANOVA

Figure 2. anti-hOX40 mIgG1 and mIgG2a mAb are costimulatory in the OT-I/hOX40KI model. A. Schematic of the experimental model; $hOX40^{het}$ OT-I cells are transferred into $hOX40KI^{hom}$ mice, immunized with OVA in the presence of anti-hOX40 mAb and various cells measured by flow cytometry before recall stimulation with SIINFEKL. B. Expansion of tetramer positive OT-I cells in $hOX40KI^{hom}$ recipients. Isotype mIgG1, anti-hOX40 mIgG1 and anti-hOX40 mIgG2a n = 4, Isotype mIgG2a n = 3, representative of two independent experiments. Numeration of OT-I (C) and Treg (D) cells in $hOX40KI^{hom}$ spleens harvested on Day 4 pooled from six independent experiments. Isotype mIgG1 and anti-hOX40 mIgG1 n = 21, isotype mIgG2a and anti-hOX40 mIgG2a n = 20, two mice per group were excluded due to no OT-I response. E. Treg fold induction pooled from six independent experiments

anti-hOX40 mIgG1 n = 21 and anti-hOX40 mIgG2a n = 20. F. As in A except hOX40^{het} OT-I purified CD8+ T cells transferred in WT C57BL/6 recipients, n = 4, representative of two independent experiments. C-E analyzed as one-way ANOVA, Sidak's multiple comparison. **** $p < 0.0001$, ** $p < 0.01$, * $p < 0.05$ Mean +/- SEM.

Figure 3. Anti-hOX40 mIgG1 mAb requires both activating and inhibitory FcγR for activity. hOX40^{het} OT-I cells were transferred into transferred into hOX40KI^{hom}, hOX40KI^{hom} γ chain KO or hOX40KI^{hom} FcγRIIB KO mice and then immunized as in Figure 2A. A. Response to anti-hOX40 mIgG1 (left panel) or anti-hOX40 mIgG2a (right panel) n = 4 except isotype mIgG2a in hOX40KI^{hom} where n = 5. One mouse was excluded from anti-hOX40 mIgG1 in hOX40KI^{hom} recipients due to a lack of OT-I response hence n = 4. Representative of two independent experiments. B. Peak OT-I responses in blood from hOX40KI^{hom} and hOX40KI^{hom} γ chain KO recipients n = 5 except Isotype mIgG1 in both hOX40KI^{hom} and hOX40KI^{hom} γ chain KO where n = 4. One of two independent experiments. Splenic analysis of OT-I (C) and CD4+Foxp3+ (D) T cells on Day 4 post OVA (5 mg) and antibody (100 μg) challenge. N = 4 except for anti-hOX40 mIgG2a in hOX40KI where n =3. One mouse excluded in isotype mIgG2a group in hOX40KI^{hom} due to lack of staining hence n = 3. Representative of two independent experiments. E. OT-I kinetic responses in hOX40KI^{hom} and hOX40KI^{hom} FcγRIIBKO mice in response to anti-hOX40 mIgG1 (left panel) or anti-hOX40 mIgG2a (right panel) n = 4 except Isotype mIgG1 in hOX40KI^{hom} and Isotype mIgG2a in hOX40KI^{hom} FcγRIIB KO mice where n = 3. Representative of two independent experiments. F-H. Splenic analysis of OT-I (F) and CD4+Foxp3+ (G) T cells on Day 4 post OVA (5 mg) and antibody (100 μg) challenge. N = 3 for all hOX40KI recipient groups, n = 4 for all hOX40KI^{hom} FcγRIIB KO except for anti-hOX40 mIgG1 and anti-hOX40 mIgG2a treated groups where one mouse was excluded as due to lack of OT-I response hence n = 3. 1 of 2 independent

experiments. H. Treg fold induction pooled from two independent experiments, n = 7 for hOX40KI^{hom} anti-hOX40 mIgG1 and mIgG2a, n = 6 for hOX40KI^{hom} FcγRIIB KO anti-hOX40 mIgG1 and mIgG2a. **** $p < 0.0001$, *** $p < 0.001$, ** $p < 0.01$, * $p < 0.05$ Mean +/- SEM B-D, and F&G – One-way ANOVA with Sidak's multiple comparison.

Figure 4. anti-hOX40 hIgG1 mAb activity requires both activating and inhibitory FcγR. hOX40^{het} OT-I cells were transferred into hOX40KI^{hom}, hOX40KI^{hom} γ chain KO or hOX40KI^{hom} FcγRIIB KO mice and then immunized as in Figure 2A. A. OT-I kinetic responses in hOX40KI^{hom} recipients in response to challenge with anti-hOX40 hIgG1, hIgG2 and hIgG4 (solid lines) or isotype controls (dashed lines) n = 3 except for Isotype hIgG4 where n = 2 due to sick mouse being culled at start of experiment. Representative of two independent experiments. Splenic analysis of OT-I (B) and CD4+Foxp3+ (C) T cells on Day 4 post OVA (5 mg) and antibody (100 μg) challenge. Isotype and anti-hOX40 hIgG1 n = 6, isotype hIgG2, anti-hOX40 hIgG2 and anti-hOX40 hIgG4 n = 5 and Isotype hIgG4 n = 4. Representative of two (B) and three (C) independent experiments. D. As in A except hOX40^{het} OT-I purified CD8+ T cells transferred in WT C57BL/6 recipients. OT-I kinetic responses in WT recipients in response to challenge with anti-hOX40 hIgG1, hIgG2 and hIgG4 (solid lines) or isotype controls (dashed lines) Isotype and anti-hOX40 hIgG1 n = 5, isotype and anti-hOX40 hIgG2 n = 4, isotype and anti-hOX40 hIgG4 n = 3. Representative of two independent experiments. E. OT-I kinetic responses in hOX40KI^{hom} and hOX40KI^{hom} γ chain KO mice in response to anti-hOX40 hIgG1, isotype hIgG1 n = 4, anti-hOX40 hIgG1 n = 3 due to one mouse excluded based on lack of OT-I response, hOX40KI^{hom} γ chain KO Isotype hIgG1 n = 5, hOX40KI^{hom} γ chain KO anti-hOX40 hIgG1 n = 4. Representative of two independent experiments. F. Splenic analysis of OT-I T cells on Day 4 post OVA (5 mg) and antibody (100 μg) challenge. hOX40KI^{hom}

Isotype hIgG1, anti-hOX40 hIgG1 and hOX40KI^{hom} γ chain KO isotype hIgG1 n = 4, hOX40KI^{hom} γ chain KO anti-hOX40 hIgG1 n = 5. G. Splenic analysis of CD4+Foxp3+ T cell fold change relative to Isotype control on Day 4 post OVA (5 mg) and antibody (100 μg) challenge. hOX40KI^{hom} anti-hOX40 hIgG1 n = 14, hOX40KI^{hom} γ chain KO anti-hOX40 hIgG1 n = 14. H. OT-I kinetic responses in hOX40KI^{hom} and hOX40KI^{hom} FcγRIIB KO mice in response to OVA and anti-OX40 hIgG1. hOX40KI^{hom} - isotype hIgG1 n = 16, OX40 hIgG1 n = 12 due to four mice being excluded based on lack of response. hOX40KI^{hom} FcγRIIB KO - isotype hIgG1 n = 19, hOX40KI^{hom} FcγRIIB KO anti-hOX40 hIgG1 n = 15 due to four mice being excluded based on lack of response. Pooled from four independent experiments. I. Blood analysis of OT-I T cells on Day 40 post OVA (5 mg) and antibody (100 μg) challenge. hOX40KI^{hom} isotype hIgG1 n = 12, hOX40KI^{hom} anti-hOX40 hIgG1 n = 10 due to two mice being excluded due to lack of response, hOX40KI^{hom} FcγRIIB KO isotype hIgG1 n = 15 and hOX40KI^{hom} FcγRIIB KO anti-hOX40 hIgG1 n = 13 due to two mice being excluded due to a lack of response, data pooled from three independent experiments. J. Splenic analysis of OT-I T cells on Day 4 post OVA (5 mg) and antibody (100 μg) challenge. hOX40KI^{hom} Isotype hIgG1 and anti-hOX40 hIgG1 n = 4, hOX40KI^{hom} FcγRIIB KO isotype hIgG1 and FcγRIIB KO anti-hOX40 hIgG1 n = 5. K. Splenic analysis of CD4+Foxp3+ T cell numbers on Day 4 post OVA (5 mg) and antibody (100 μg) challenge. hOX40KI^{hom} Isotype hIgG1 n = 4, anti-hOX40 hIgG1 n = 6, hOX40KI^{hom} FcγRIIB KO isotype hIgG1 n = 4 and hOX40KI^{hom} FcγRIIB KO anti-hOX40 hIgG1 n = 6. L. Splenic analysis of CD4+Foxp3+ T cell fold change relative to isotype control on Day 4 post OVA (5 mg) and antibody (100 μg) challenge. hOX40KI^{hom} n = 10, hOX40KI^{hom} FcγRIIB KO n = 11 data pooled from two independent experiments. **** $p < 0.0001$, ** $p < 0.01$, * $p < 0.05$ Mean +/- SEM B-C, F & J– Sidak's multiple comparison one-way ANOVA, G – unpaired T-Test, I – Tukey's multiple comparison one-way ANOVA

Figure 5. Combination of anti-hOX40 and anti-PD-1 is more efficacious than monotherapy. A. Schematic of treatment regime used in B-D. B. Growth curves of hOX40KI^{hom} mice inoculated with 0.5x10^{6} E.G7-OVA S.C. and then treated with 100 μg anti-hOX40 mIgG1 or mIgG2a or respective isotype controls on Day 10, 13, 16. N = 9 representative of three independent experiments. C. Survival graph of hOX40KI^{hom} mice challenged as in B. Isotype mIgG1 n = 21, isotype mIgG2a n = 20, anti-hOX40 mIgG1 n = 19 and anti-hOX40 mIgG2a n = 19 pooled from three independent experiments. D. Growth curves of hOX40KI^{hom} mice inoculated with 0.5x10^{6} E.G7-OVA S.C. and then treated with 100 μg anti-hOX40 hIgG1, hIgG2 or hIgG4 or respective isotype controls on Day 10, 13, 16. Isotype hIgG1 n = 4, isotype hIgG2 n = 7, isotype hIgG4 n = 6, anti-hOX40 hIgG1 n = 7, anti-hOX40 hIgG2 n = 5 and anti-hOX40 hIgG4 n = 6, representative of two independent experiments. E. Survival graph of hOX40KI^{hom} mice challenged as in D. Isotype hIgG1 n = 8, isotype hIgG2 n = 12, isotype hIgG4 n = 11, anti-hOX40 hIgG1 n = 14, anti-hOX40 hIgG2 n =10 and anti-hOX40 hIgG4 n =12 pooled from two independent experiments. F. Schematic of E.G7-OVA tumors treated with anti-OX40 and anti-PD-1. G. Growth curves of hOX40KI^{hom} mice inoculated with 0.5x10^{6} E.G7-OVA S.C. and then treated as detailed in F. Isotype combination n = 8, anti-hOX40 hIgG1 n = 8, anti-PD-1 rIgG2a n = 8 and anti-hOX40 hIgG1 + anti-PD-1 rIgG2a n = 7, representative of two independent experiments. H. Survival plots of hOX40KI mice challenged as in F. Isotype combination n = 15, anti-hOX40 hIgG1 n = 14, anti-PD-1 rIgG2a n = 14 and OX40 hIgG1 + anti-PD-1 rIgG2a n = 13. **** $p < 0.0001$, ** $p < 0.01$, * $p < 0.05$ Mean +/- SEM B - Sidak's multiple comparison one-way ANOVA on day 52 related to isotype control, C, E and H – log-rank test.

Figure 6. anti-hOX40 and anti-PD-1 combination increases cytokine production from hPBMC cultures. A. Resected tumor samples were analyzed for CD4, CD8 and Treg populations n = 45 for CD4 and CD8 and n = 39 for Treg. B. hOX40 expression on resected tumor samples on CD4+ effectors, Tregs and CD8+ T cells, n = 12. C. hOX40 receptor density on resected tumor samples was determined using BDBioscience Quantibrite beads n = 13. D. Analysis of total OX40 receptor numbers/cell in healthy donor (filled circles) and patient (open circles) PBMCS activated for 2 days with anti-CD3/anti-CD28 beads n = 10. E. Fold induction of FcγRIII ADCC following healthy (filled circles) and patient (open circles) PBMCs activation for 2 days with anti-CD3/anti-CD28 beads, separation into cell type and then incubated with 10 μg/ml anti-OX40 (GSK3174998), n = 10. F Correlation of total hOX40 receptor numbers (as determined by numbers of hOX40 receptors per cell x % hOX40+ cells) with ADCC fold induction in response to anti-hOX40 treatment of cells isolated from healthy and patient donors activated as in D & E. n = 10. **** $p < 0.0001$, *** $p < 0.001$, ** $p < 0.01$, * $p<0.05$ Mean +/- SEM B-E – Tukey's multiple comparison one-way ANOVA F - Pearson correlation.

References:

1. Couzin-Frankel J. Breakthrough of the year 2013. Cancer immunotherapy. Science. 2013;342(6165):1432-3.
2. Ribas A, Wolchok JD. Cancer immunotherapy using checkpoint blockade. Science. 2018;359(6382):1350-5.
3. Kalbasi A, Ribas A. Tumour-intrinsic resistance to immune checkpoint blockade. Nat Rev Immunol. 2020;20(1):25-39.
4. Kubli SP, Berger T, Araujo DV, Siu LL, Mak TW. Beyond immune checkpoint blockade: emerging immunological strategies. Nat Rev Drug Discov. 2021;20(12):899-919.
5. Sharma P, Hu-Lieskovan S, Wargo JA, Ribas A. Primary, Adaptive, and Acquired Resistance to Cancer Immunotherapy. Cell. 2017;168(4):707-23.
6. Alves Costa Silva C, Facchinetti F, Routy B, Derosa L. New pathways in immune stimulation: targeting OX40. ESMO Open. 2020;5(1).
7. Aspeslagh S, Postel-Vinay S, Rusakiewicz S, Soria JC, Zitvogel L, Marabelle A. Rationale for anti-OX40 cancer immunotherapy. Eur J Cancer. 2016;52:50-66.

8. Deng J, Zhao S, Zhang X, Jia K, Wang H, Zhou C, He Y. OX40 (CD134) and OX40 ligand, important immune checkpoints in cancer. Onco Targets Ther. 2019;12:7347-53.
9. Buchan SL, Rogel A, Al-Shamkhani A. The immunobiology of CD27 and OX40 and their potential as targets for cancer immunotherapy. Blood. 2018;131(1):39-48.
10. Weinberg AD, Morris NP, Kovacsovics-Bankowski M, Urba WJ, Curti BD. Science gone translational: the OX40 agonist story. Immunol Rev. 2011;244(1):218-31.
11. Rogers PR, Song J, Gramaglia I, Killeen N, Croft M. OX40 promotes Bcl-xL and Bcl-2 expression and is essential for long-term survival of CD4 T cells. Immunity. 2001;15(3):445-55.
12. Song J, So T, Cheng M, Tang X, Croft M. Sustained survivin expression from OX40 costimulatory signals drives T cell clonal expansion. Immunity. 2005;22(5):621-31.
13. Voo KS, Bover L, Harline ML, Vien LT, Facchinetti V, Arima K, et al. Antibodies targeting human OX40 expand effector T cells and block inducible and natural regulatory T cell function. J Immunol. 2013;191(7):3641-50.
14. Willoughby J, Griffiths J, Tews I, Cragg MS. OX40: Structure and function - What questions remain? Mol Immunol. 2017;83:13-22.
15. Gough MJ, Ruby CE, Redmond WL, Dhungel B, Brown A, Weinberg AD. OX40 agonist therapy enhances CD8 infiltration and decreases immune suppression in the tumor. Cancer Res. 2008;68(13):5206-15.
16. Griffiths J, Hussain K, Smith HL, Sanders T, Cox KL, Semmrich M, et al. Domain binding and isotype dictate the activity of anti-human OX40 antibodies. J Immunother Cancer. 2020;8(2).
17. Jensen SM, Maston LD, Gough MJ, Ruby CE, Redmond WL, Crittenden M, et al. Signaling through OX40 enhances antitumor immunity. Semin Oncol. 2010;37(5):524-32.
18. Linch SN, McNamara MJ, Redmond WL. OX40 Agonists and Combination Immunotherapy: Putting the Pedal to the Metal. Front Oncol. 2015;5:34.
19. Turaj AH, Cox KL, Penfold CA, French RR, Mockridge CI, Willoughby JE, et al. Augmentation of CD134 (OX40)-dependent NK anti-tumour activity is dependent on antibody cross-linking. Sci Rep. 2018;8(1):2278.
20. Yadav R, Redmond WL. Current Clinical Trial Landscape of OX40 Agonists. Curr Oncol Rep. 2022;24(7):951-60.
21. Gutierrez M, Moreno V, Heinhuis KM, Olszanski AJ, Spreafico A, Ong M, et al. OX40 Agonist BMS-986178 Alone or in Combination With Nivolumab and/or Ipilimumab in Patients With Advanced Solid Tumors. Clin Cancer Res. 2021;27(2):460-72.
22. Ma Y, Li J, Wang H, Chiu Y, Kingsley CV, Fry D, et al. Combination of PD-1 Inhibitor and OX40 Agonist Induces Tumor Rejection and Immune Memory in Mouse Models of Pancreatic Cancer. Gastroenterology. 2020;159(1):306-19 e12.
23. Messenheimer DJ, Jensen SM, Afentoulis ME, Wegmann KW, Feng Z, Friedman DJ, et al. Timing of PD-1 Blockade Is Critical to Effective Combination Immunotherapy with Anti-OX40. Clin Cancer Res. 2017;23(20):6165-77.
24. Shrimali RK, Ahmad S, Verma V, Zeng P, Ananth S, Gaur P, et al. Concurrent PD-1 Blockade Negates the Effects of OX40 Agonist Antibody in Combination Immunotherapy through Inducing T-cell Apoptosis. Cancer Immunol Res. 2017;5(9):755-66.

25. Wang R, Gao C, Raymond M, Dito G, Kabbabe D, Shao X, et al. An Integrative Approach to Inform Optimal Administration of OX40 Agonist Antibodies in Patients with Advanced Solid Tumors. Clin Cancer Res. 2019;25(22):6709-20.
26. Postel-Vinay S, Lam VK, Ros W, Bauer TM, Hansen AR, Cho DC, et al. First-in-human phase I study of the OX40 agonist GSK3174998 with or without pembrolizumab in patients with selected advanced solid tumors (ENGAGE-1). J Immunother Cancer. 2023;11(3).
27. Bulliard Y, Jolicoeur R, Zhang J, Dranoff G, Wilson NS, Brogdon JL. OX40 engagement depletes intratumoral Tregs via activating FcgammaRs, leading to antitumor efficacy. Immunol Cell Biol. 2014;92(6):475-80.
28. Campos Carrascosa L, van Beek AA, de Ruiter V, Doukas M, Wei J, Fisher TS, et al. FcgammaRIIB engagement drives agonistic activity of Fc-engineered alphaOX40 antibody to stimulate human tumor-infiltrating T cells. J Immunother Cancer. 2020;8(2).
29. Dahan R, Sega E, Engelhardt J, Selby M, Korman AJ, Ravetch JV. FcgammaRs Modulate the Anti-tumor Activity of Antibodies Targeting the PD-1/PD-L1 Axis. Cancer Cell. 2015;28(3):285-95.
30. Moreno-Vicente J, Willoughby JE, Taylor MC, Booth SG, English VL, Williams EL, et al. Fc-null anti-PD-1 monoclonal antibodies deliver optimal checkpoint blockade in diverse immune environments. J Immunother Cancer. 2022;10(1).
31. Zhang T, Song X, Xu L, Ma J, Zhang Y, Gong W, et al. The binding of an anti-PD-1 antibody to FcgammaRIota has a profound impact on its biological functions. Cancer Immunol Immunother. 2018;67(7):1079-90.
32. al-Shamkhani A, Birkeland ML, Puklavec M, Brown MH, James W, Barclay AN. OX40 is differentially expressed on activated rat and mouse T cells and is the sole receptor for the OX40 ligand. Eur J Immunol. 1996;26(8):1695-9.
33. Chu F, Li HS, Liu X, Cao J, Ma W, Ma Y, et al. CXCR5(+)CD8(+) T cells are a distinct functional subset with an antitumor activity. Leukemia. 2019;33(11):2640-53.
34. Polesso F, Weinberg AD, Moran AE. Late-Stage Tumor Regression after PD-L1 Blockade Plus a Concurrent OX40 Agonist. Cancer Immunol Res. 2019;7(2):269-81.
35. Jackson H, Bhattacharya S, Bojczuk P, Kilian D, Seestaller Wehr L, Hahn A, et al. 1192P - Evaluation of OX40 receptor density, influence of IgG Isotype and dosing paradigm in anti-OX40-mediated efficacy and biomarker responses with PD-1 blockade. Annals of Oncology. 2018;29:viii424-viii5.
36. Stewart R, Hammond SA, Oberst M, Wilkinson RW. The role of Fc gamma receptors in the activity of immunomodulatory antibodies for cancer. Journal for ImmunoTherapy of Cancer. 2014;2(1):29.
37. Temming AR, Bentlage AEH, de Taeye SW, Bosman GP, Lissenberg-Thunnissen SN, Derksen NIL, et al. Cross-reactivity of mouse IgG subclasses to human Fc gamma receptors: Antibody deglycosylation only eliminates IgG2b binding. Mol Immunol. 2020;127:79-86.
38. Beers SA, Glennie MJ, White AL. Influence of immunoglobulin isotype on therapeutic antibody function. Blood. 2016;127(9):1097-101.
39. Buchan SL, Dou L, Remer M, Booth SG, Dunn SN, Lai C, et al. Antibodies to Costimulatory Receptor 4-1BB Enhance Anti-tumor Immunity via T Regulatory Cell Depletion and Promotion of CD8 T Cell Effector Function. Immunity. 2018;49(5):958-70 e7.

40. Li F, Ravetch JV. A general requirement for FcgammaRIIB co-engagement of agonistic anti-TNFR antibodies. Cell Cycle. 2012;11(18):3343-4.
41. White AL, Chan HT, French RR, Beers SA, Cragg MS, Johnson PW, Glennie MJ. FcgammaRIotaIotaB controls the potency of agonistic anti-TNFR mAbs. Cancer Immunol Immunother. 2013;62(5):941-8.
42. Beers SA, French RR, Chan HT, Lim SH, Jarrett TC, Vidal RM, et al. Antigenic modulation limits the efficacy of anti-CD20 antibodies: implications for antibody selection. Blood. 2010;115(25):5191-201.
43. Nimmerjahn F, Ravetch JV. Divergent immunoglobulin g subclass activity through selective Fc receptor binding. Science. 2005;310(5753):1510-2.
44. Verma V, Shrimali RK, Ahmad S, Dai W, Wang H, Lu S, et al. PD-1 blockade in subprimed CD8 cells induces dysfunctional PD-1(+)CD38(hi) cells and anti-PD-1 resistance. Nat Immunol. 2019;20(9):1231-43.
45. Arce Vargas F, Furness AJS, Litchfield K, Joshi K, Rosenthal R, Ghorani E, et al. Fc Effector Function Contributes to the Activity of Human Anti-CTLA-4 Antibodies. Cancer Cell. 2018;33(4):649-63 e4.
46. Freeman ZT, Nirschl TR, Hovelson DH, Johnston RJ, Engelhardt JJ, Selby MJ, et al. A conserved intratumoral regulatory T cell signature identifies 4-1BB as a pan-cancer target. J Clin Invest. 2020;130(3):1405-16.
47. Montler R, Bell RB, Thalhofer C, Leidner R, Feng Z, Fox BA, et al. OX40, PD-1 and CTLA-4 are selectively expressed on tumor-infiltrating T cells in head and neck cancer. Clin Transl Immunology. 2016;5(4):e70.
48. Wasiuk A, Testa J, Weidlick J, Sisson C, Vitale L, Widger J, et al. CD27-Mediated Regulatory T Cell Depletion and Effector T Cell Costimulation Both Contribute to Antitumor Efficacy. J Immunol. 2017;199(12):4110-23.
49. Hussain K, Hargreaves CE, Roghanian A, Oldham RJ, Chan HT, Mockridge CI, et al. Upregulation of FcgammaRIIb on monocytes is necessary to promote the superagonist activity of TGN1412. Blood. 2015;125(1):102-10.
50. White AL, Chan HT, Roghanian A, French RR, Mockridge CI, Tutt AL, et al. Interaction with FcgammaRIIB is critical for the agonistic activity of anti-CD40 monoclonal antibody. J Immunol. 2011;187(4):1754-63.
51. Bruhns P, Jonsson F. Mouse and human FcR effector functions. Immunol Rev. 2015;268(1):25-51.
52. Dekkers G, Bentlage AEH, Stegmann TC, Howie HL, Lissenberg-Thunnissen S, Zimring J, et al. Affinity of human IgG subclasses to mouse Fc gamma receptors. MAbs. 2017;9(5):767-73.
53. Chan FK, Chun HJ, Zheng L, Siegel RM, Bui KL, Lenardo MJ. A domain in TNF receptors that mediates ligand-independent receptor assembly and signaling. Science. 2000;288(5475):2351-4.
54. Waight JD, Chand D, Dietrich S, Gombos R, Horn T, Gonzalez AM, et al. Selective FcgammaR Co-engagement on APCs Modulates the Activity of Therapeutic Antibodies Targeting T Cell Antigens. Cancer Cell. 2018;33(6):1033-47 e5.
55. Yofe I, Landsberger T, Yalin A, Solomon I, Costoya C, Demane DF, et al. Anti-CTLA-4 antibodies drive myeloid activation and reprogram the tumor microenvironment through FcgammaR engagement and type I interferon signaling. Nat Cancer. 2022;3(11):1336-50.
56. Lim SH, Beers SA, Al-Shamkhani A, Cragg MS. Agonist antibodies for cancer immunotherapy: History, Hopes and Challenges. Clin Cancer Res. 2023.

57. Orr CM, Fisher H, Yu X, Chan CH, Gao Y, Duriez PJ, et al. Hinge disulfides in human IgG2 CD40 antibodies modulate receptor signaling by regulation of conformation and flexibility. Sci Immunol. 2022;7(73):eabm3723.
58. Yu X, James S, Felce JH, Kellermayer B, Johnston DA, Chan HTC, et al. TNF receptor agonists induce distinct receptor clusters to mediate differential agonistic activity. Commun Biol. 2021;4(1):772.
59. Davis EJ, Martin-Liberal J, Kristeleit R, Cho DC, Blagden SP, Berthold D, et al. First-in-human phase I/II, open-label study of the anti-OX40 agonist INCAGN01949 in patients with advanced solid tumors. J Immunother Cancer. 2022;10(10).
60. Diab A, Hamid O, Thompson JA, Ros W, Eskens F, Doi T, et al. A Phase I, Open-Label, Dose-Escalation Study of the OX40 Agonist Ivuxolimab in Patients with Locally Advanced or Metastatic Cancers. Clin Cancer Res. 2022;28(1):71-83.
61. Kim TW, Burris HA, de Miguel Luken MJ, Pishvaian MJ, Bang YJ, Gordon M, et al. First-In-Human Phase I Study of the OX40 Agonist MOXR0916 in Patients with Advanced Solid Tumors. Clin Cancer Res. 2022;28(16):3452-63.
62. Hussain K, Liu R, Smith RCG, Muller KTJ, Ghorbani M, Macari S, et al. HIF activation enhances FcgammaRIIb expression on mononuclear phagocytes impeding tumor targeting antibody immunotherapy. J Exp Clin Cancer Res. 2022;41(1):131.
63. Dees S, Ganesan R, Singh S, Grewal IS. Regulatory T cell targeting in cancer: Emerging strategies in immunotherapy. Eur J Immunol. 2021;51(2):280-91.
64. Sharma A, Subudhi SK, Blando J, Scutti J, Vence L, Wargo J, et al. Anti-CTLA-4 Immunotherapy Does Not Deplete FOXP3(+) Regulatory T Cells (Tregs) in Human Cancers. Clin Cancer Res. 2019;25(4):1233-8.
65. Quezada SA, Peggs KS. Lost in Translation: Deciphering the Mechanism of Action of Anti-human CTLA-4. Clin Cancer Res. 2019;25(4):1130-2.
66. Liu R, Oldham RJ, Teal E, Beers SA, Cragg MS. Fc-Engineering for Modulated Effector Functions-Improving Antibodies for Cancer Treatment. Antibodies (Basel). 2020;9(4).

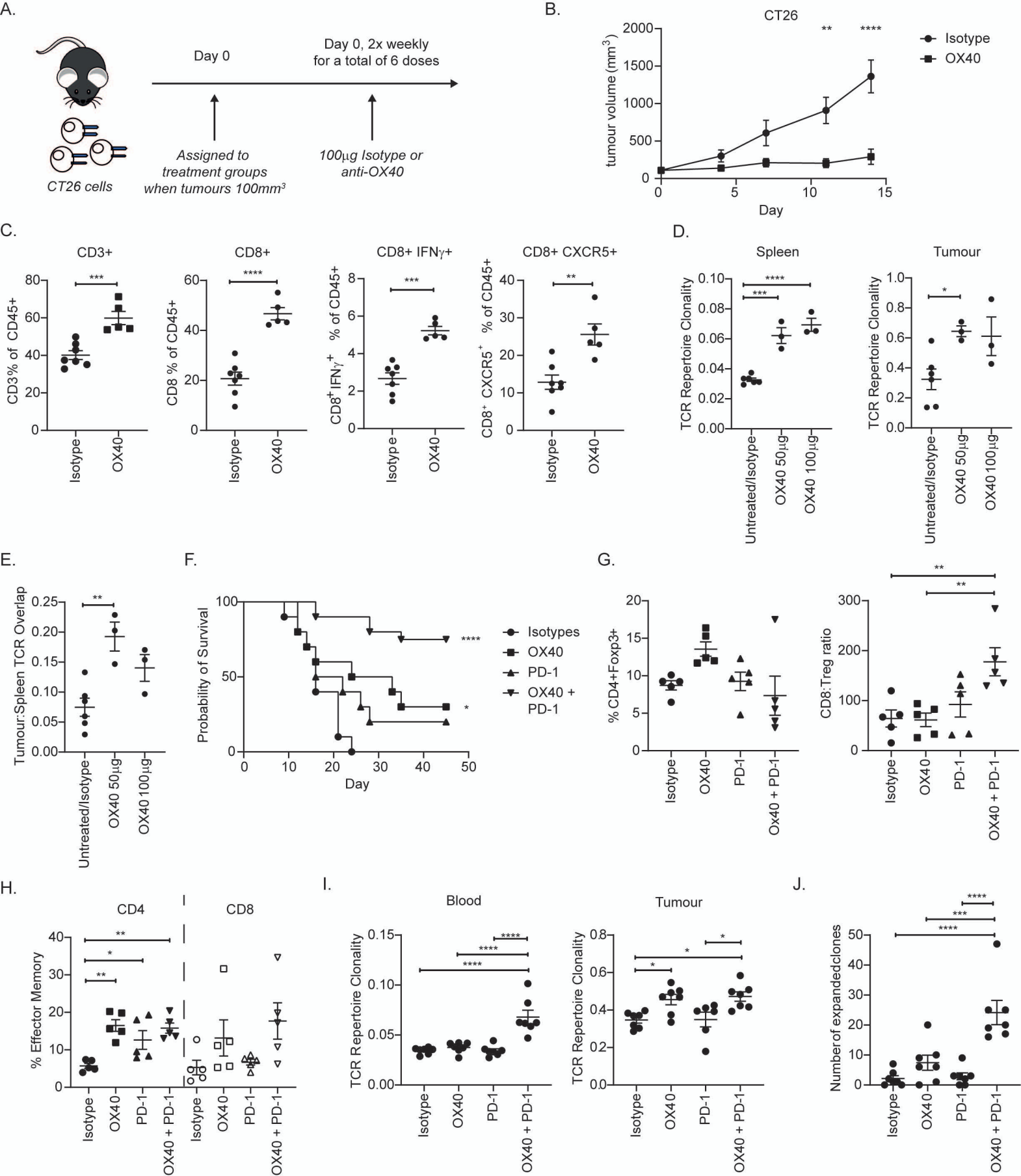
A.
Day 0
Day 0, 2x weekly for a total of 6 doses
CT26 cells
Assigned to treatment groups when tumours 100mm3
100μg Isotype or anti-OX40
B.
CT26
tumour volume (mm3)
Day
Isotype
OX40
C.
CD3+
CD8+
CD8+ IFNγ+
CD8+ CXCR5+
D.
Spleen
Tumour
TCR Repertoire Clonality
Untreated/Isotype
OX40 50μg
OX40 100μg
E.
Tumour:Spleen TCR Overlap
F.
Probability of Survival
Day
Isotypes
OX40
PD-1
OX40 + PD-1
G.
% CD4+Foxp3+
CD8:Treg ratio
H.
CD4
CD8
% Effector Memory
I.
Blood
Tumour
J.
Number of expanded clones

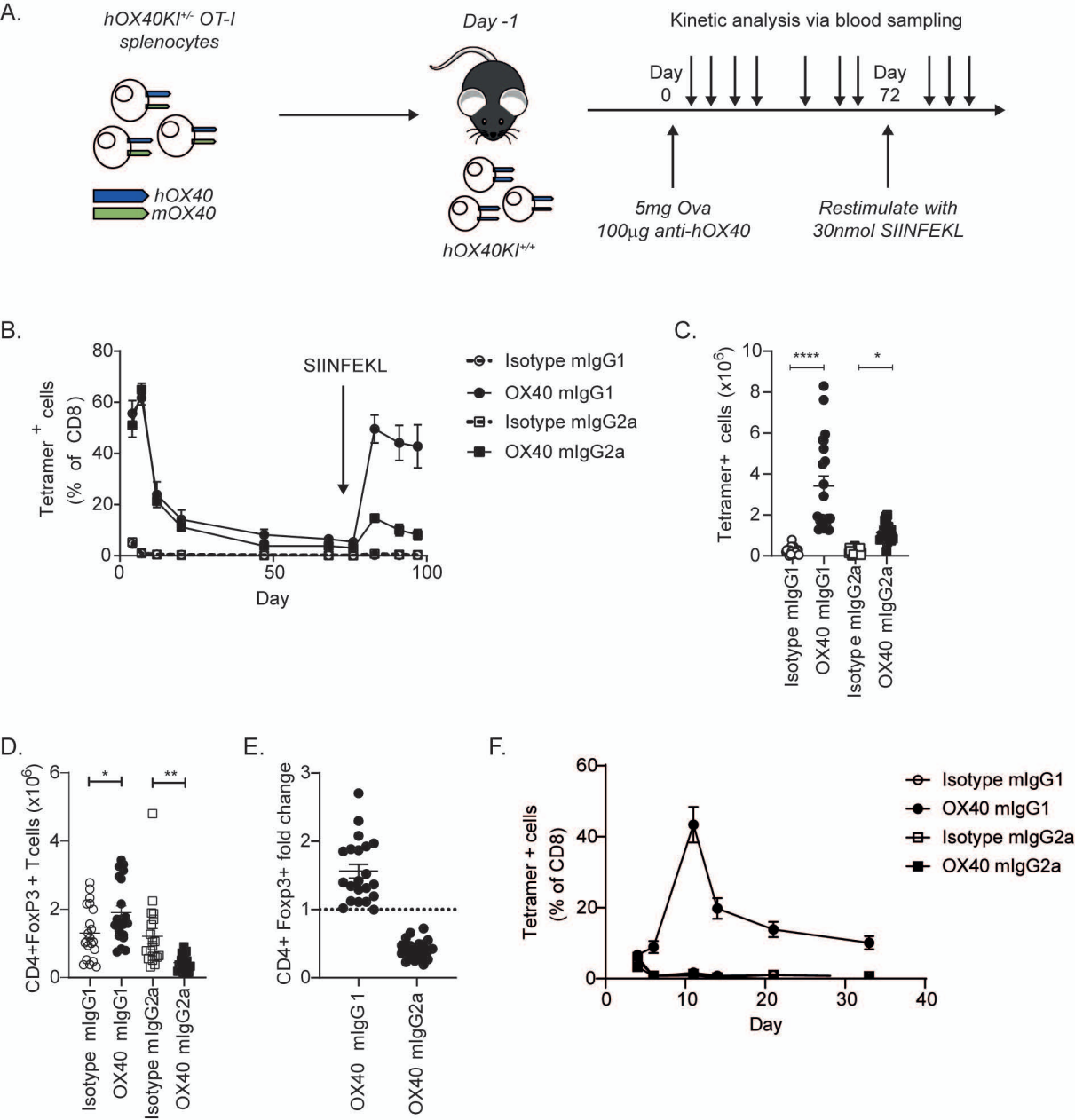
A.
hOX40KI+/- OT-I splenocytes
hOX40
mOX40
Day -1
hOX40KI+/+
Kinetic analysis via blood sampling
Day 0
Day 72
5mg Ova
100μg anti-hOX40
Restimulate with
30nmol SIINFEKL
B.
Tetramer+ cells (% of CD8)
SIINFEKL
Day
Isotype mIgG1
OX40 mIgG1
Isotype mIgG2a
OX40 mIgG2a
C.
Tetramer+ cells (x10^6)
****
*
Isotype mIgG1
OX40 mIgG1
Isotype mIgG2a
OX40 mIgG2a
D.
CD4+FoxP3 + T cells (x10^6)
*
**
Isotype mIgG1
OX40 mIgG1
Isotype mIgG2a
OX40 mIgG2a
E.
CD4+ Foxp3+ fold change
OX40 mIgG1
OX40 mIgG2a
F.
Tetramer + cells (% of CD8)
Day
Isotype mIgG1
OX40 mIgG1
Isotype mIgG2a
OX40 mIgG2a

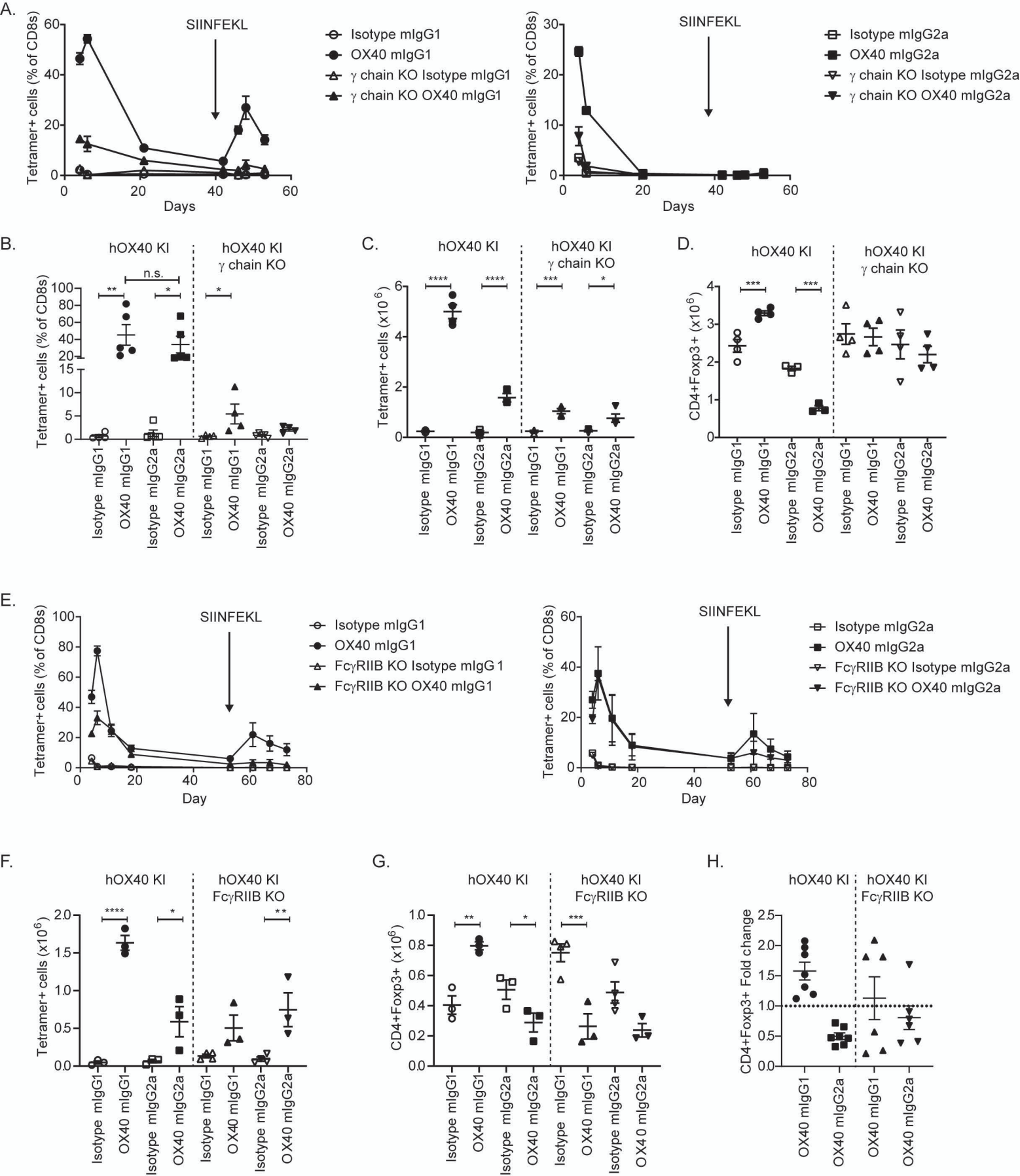
A.
SIINFEKL
Tetramer+ cells (% of CD8s)
Days
Isotype mIgG1
OX40 mIgG1
γ chain KO Isotype mIgG1
γ chain KO OX40 mIgG1
Isotype mIgG2a
OX40 mIgG2a
γ chain KO Isotype mIgG2a
γ chain KO OX40 mIgG2a
B.
hOX40 KI
hOX40 KI γ chain KO
n.s.
C.
Tetramer+ cells (x10^6)
D.
CD4+Foxp3+ (x10^6)
E.
Day
FcγRIIB KO Isotype mIgG1
FcγRIIB KO OX40 mIgG1
FcγRIIB KO Isotype mIgG2a
FcγRIIB KO OX40 mIgG2a
F.
hOX40 KI FcγRIIB KO
G.
CD4+Foxp3+ (x10^6)
H.
CD4+Foxp3+ Fold change

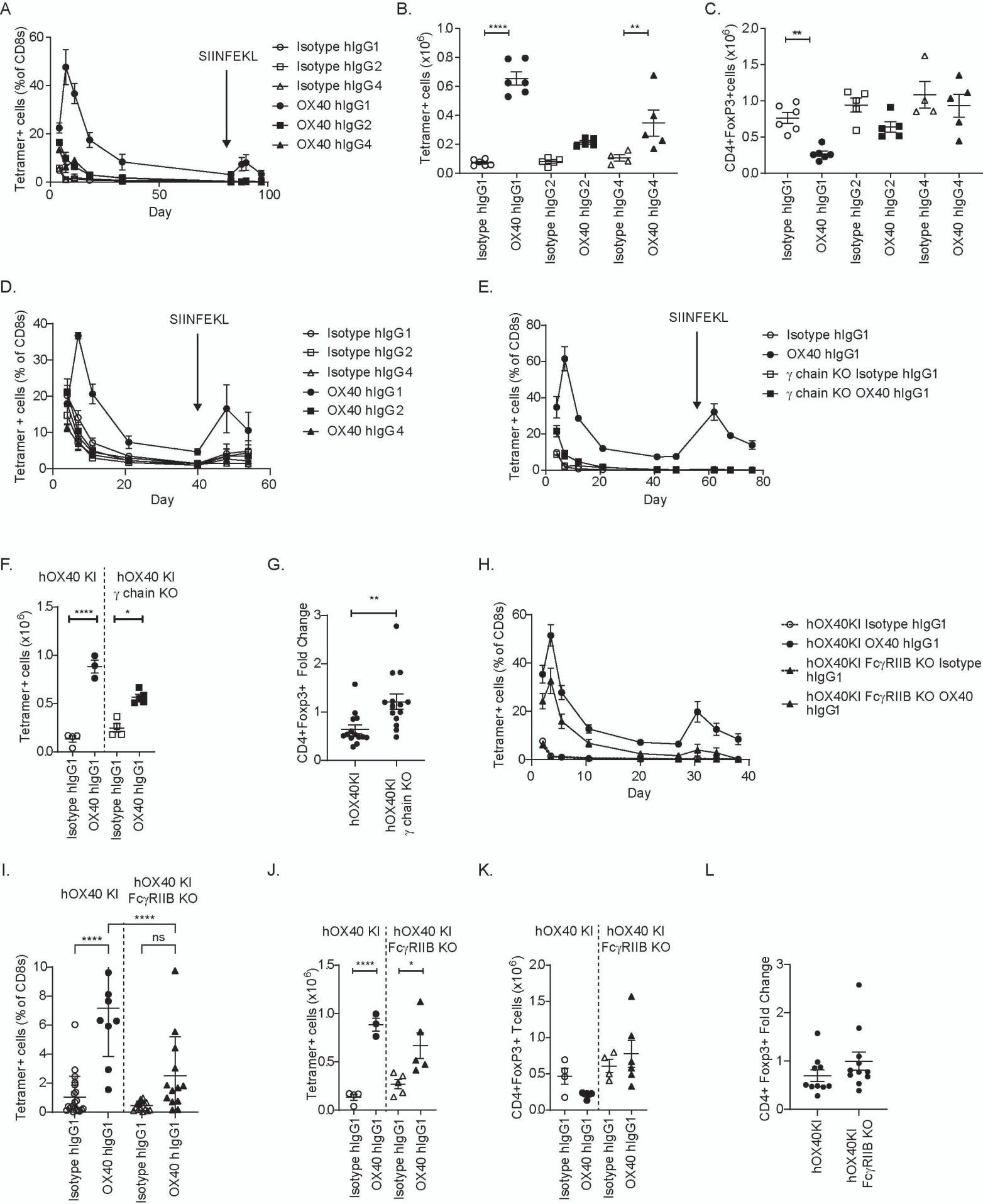
A
Tetramer+ cells (%of CD8s)
Day
SIINFEKL
Isotype hIgG1
Isotype hIgG2
Isotype hIgG4
OX40 hIgG1
OX40 hIgG2
OX40 hIgG4
B.
Tetramer+ cells (x10^6)
****
**
Isotype hIgG1
OX40 hIgG1
Isotype hIgG2
OX40 hIgG2
Isotype hIgG4
OX40 hIgG4
C.
CD4+FoxP3+cells (x10^6)
**
D.
Tetramer + cells (% of CD8s)
Day
SIINFEKL
E.
Tetramer + cells (% of CD8s)
Day
SIINFEKL
γ chain KO Isotype hIgG1
γ chain KO OX40 hIgG1
F.
hOX40 KI
hOX40 KI γ chain KO
Tetramer+ cells (x10^6)
G.
CD4+Foxp3+ Fold Change
hOX40KI
hOX40KI γ chain KO
H.
Tetramer+ cells (% of CD8s)
Day
hOX40KI Isotype hIgG1
hOX40KI OX40 hIgG1
hOX40KI FcγRIIB KO Isotype hIgG1
hOX40KI FcγRIIB KO OX40 hIgG1
I.
hOX40 KI
hOX40 KI FcγRIIB KO
Tetramer+ cells (% of CD8s)
ns
J.
hOX40 KI
hOX40 KI FcγRIIB KO
Tetramer+ cells (x10^6)
K.
hOX40 KI
hOX40 KI FcγRIIB KO
CD4+FoxP3+ Tcells (x10^6)
L
CD4+ Foxp3+ Fold Change
hOX40KI
hOX40KI FcγRIIB KO

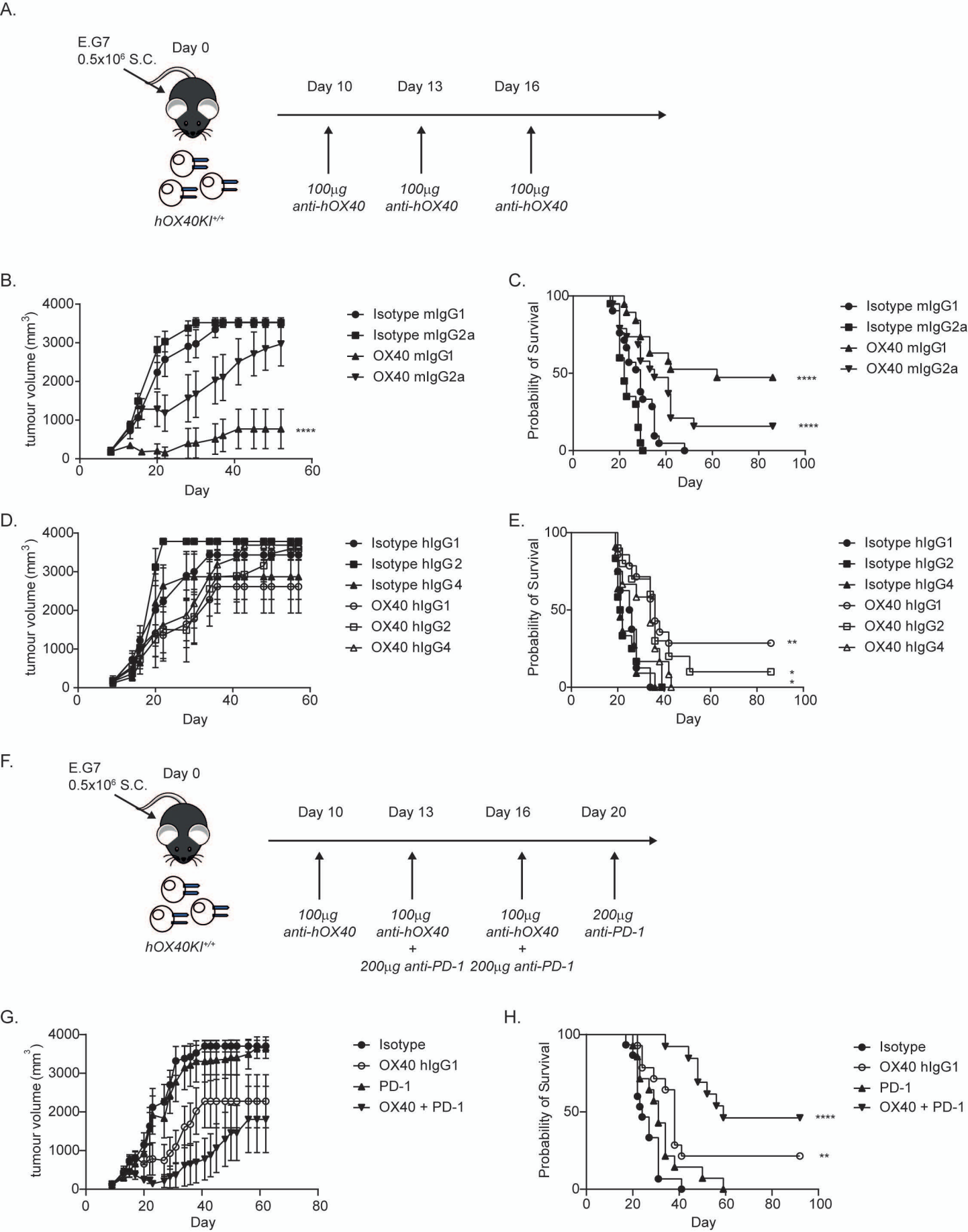
A.
E.G7
0.5x10⁶ S.C.
Day 0
hOX40KI+/+
Day 10
Day 13
Day 16
100μg anti-hOX40
100μg anti-hOX40
100μg anti-hOX40
B.
tumour volume (mm3)
Day
Isotype mIgG1
Isotype mIgG2a
OX40 mIgG1
OX40 mIgG2a
****
C.
Probability of Survival
Day
Isotype mIgG1
Isotype mIgG2a
OX40 mIgG1
OX40 mIgG2a
****
****
D.
tumour volume (mm3)
Day
Isotype hIgG1
Isotype hIgG2
Isotype hIgG4
OX40 hIgG1
OX40 hIgG2
OX40 hIgG4
E.
Probability of Survival
Day
Isotype hIgG1
Isotype hIgG2
Isotype hIgG4
OX40 hIgG1
OX40 hIgG2
OX40 hIgG4
**
*
*
F.
E.G7
0.5x10⁶ S.C.
Day 0
hOX40KI+/+
Day 10
Day 13
Day 16
Day 20
100μg anti-hOX40
100μg anti-hOX40 + 200μg anti-PD-1
100μg anti-hOX40 + 200μg anti-PD-1
200μg anti-PD-1
G.
tumour volume (mm3)
Day
Isotype
OX40 hIgG1
PD-1
OX40 + PD-1
H.
Probability of Survival
Day
Isotype
OX40 hIgG1
PD-1
OX40 + PD-1
****
**

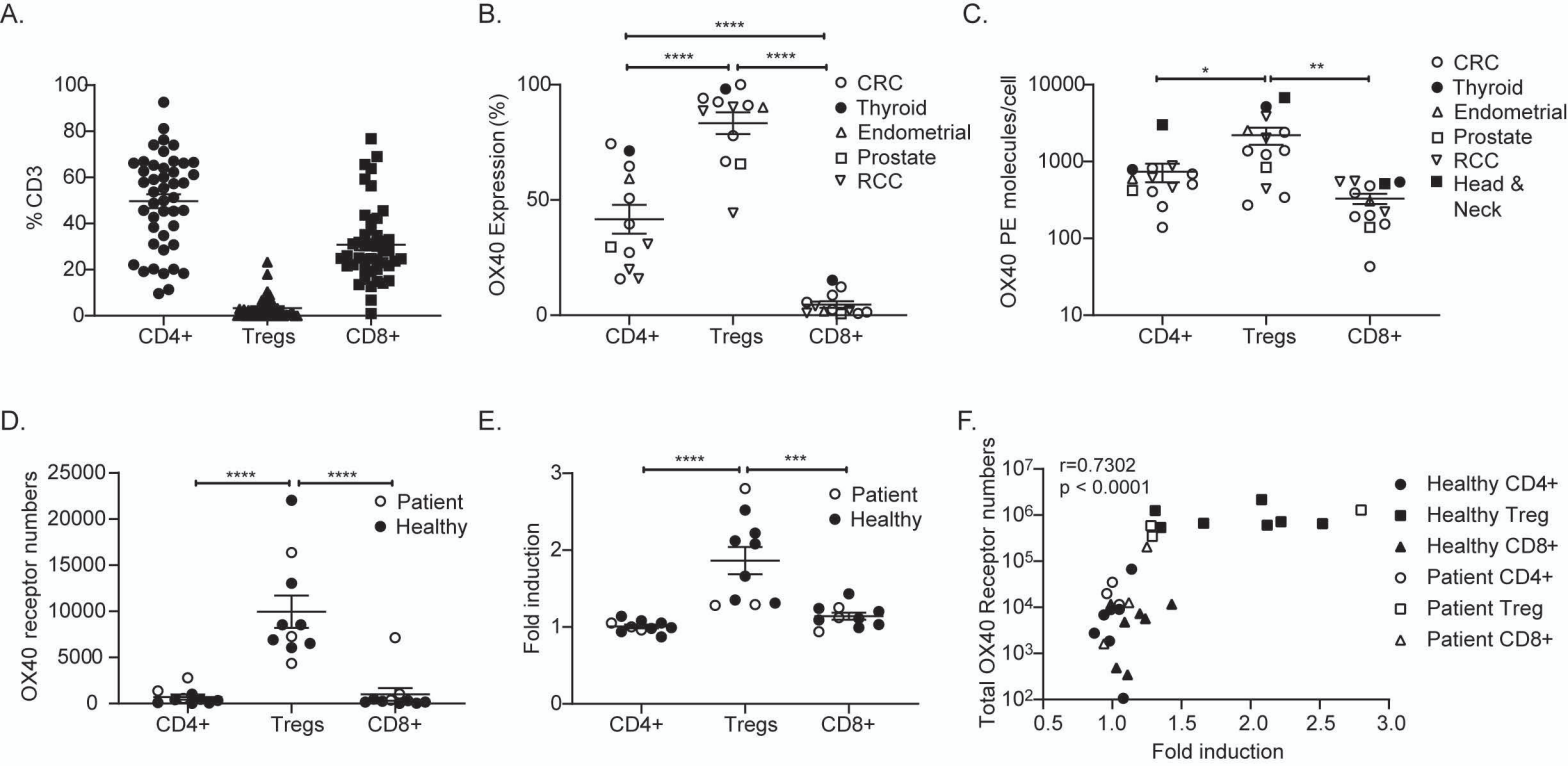
A.
% CD3
100
80
60
40
20
0
CD4+
Tregs
CD8+
B.
OX40 Expression (%)
****
****
****
100
50
0
CRC
Thyroid
Endometrial
Prostate
RCC
CD4+
Tregs
CD8+
C.
OX40 PE molecules/cell
*
**
10000
1000
100
10
CRC
Thyroid
Endometrial
Prostate
RCC
Head & Neck
CD4+
Tregs
CD8+
D.
OX40 receptor numbers
****
****
25000
20000
15000
10000
5000
0
Patient
Healthy
CD4+
Tregs
CD8+
E.
Fold induction
****
***
3
2
1
0
Patient
Healthy
CD4+
Tregs
CD8+
F.
Total OX40 Receptor numbers
r=0.7302
p < 0.0001
10^7
10^6
10^5
10^4
10^3
10^2
0.5
1.0
1.5
2.0
2.5
3.0
Fold induction
Healthy CD4+
Healthy Treg
Healthy CD8+
Patient CD4+
Patient Treg
Patient CD8+

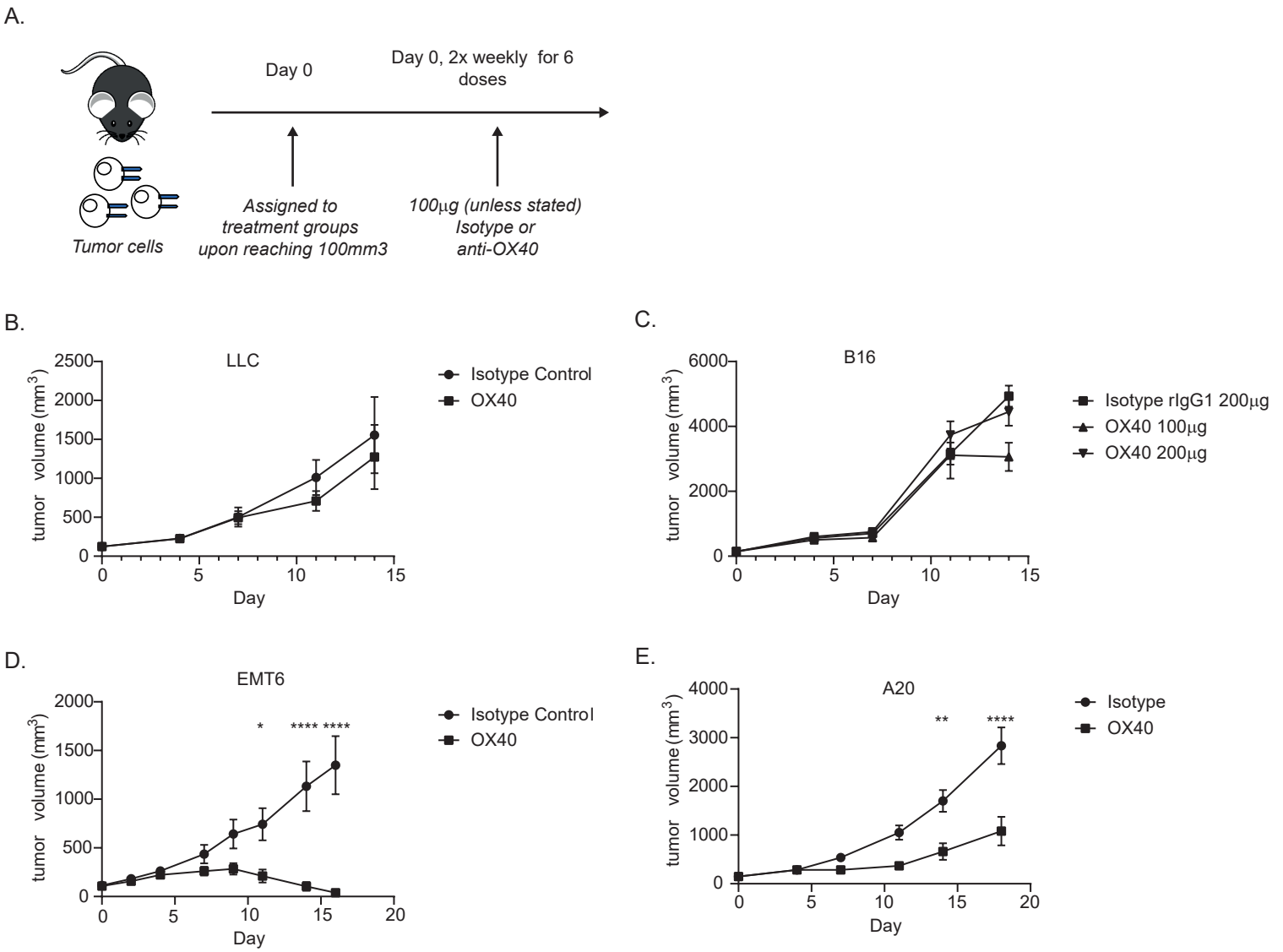

Supplemental Fig 1. A. Schematic for experiments shown in B-F. Mice were challenged with tumour cells, assigned to treatment groups upon reaching 100mm^3 and treated with either isotype control or anti-OX40. B. Growth curves for mice challenged with LLC (1x10^5 cells) and treated with 100 μg n= 7, one experiment. C. Growth curves of mice challenged with B16F10 (2.5x10^4 cells) and treated with either 100 μg or 200 μg OX40. n=6 for Isotype rIgG1 and n=7 for both OX40 groups, one experiment. D. Growth curves of EMT6 (1x10^5) and treated with 100 μg n=10 one experiment. E. Growth curves of mice challenged with A20 (1x10^6) and treated with 100 μg OX40. n=25 isotype control and n=26 anti-OX40 one experiment. **** $p < 0.0001$, ** $p < 0.01$, * $p < 0.05$ Mean +/- SEM Sidak's multiple comparison one-way ANOVA.

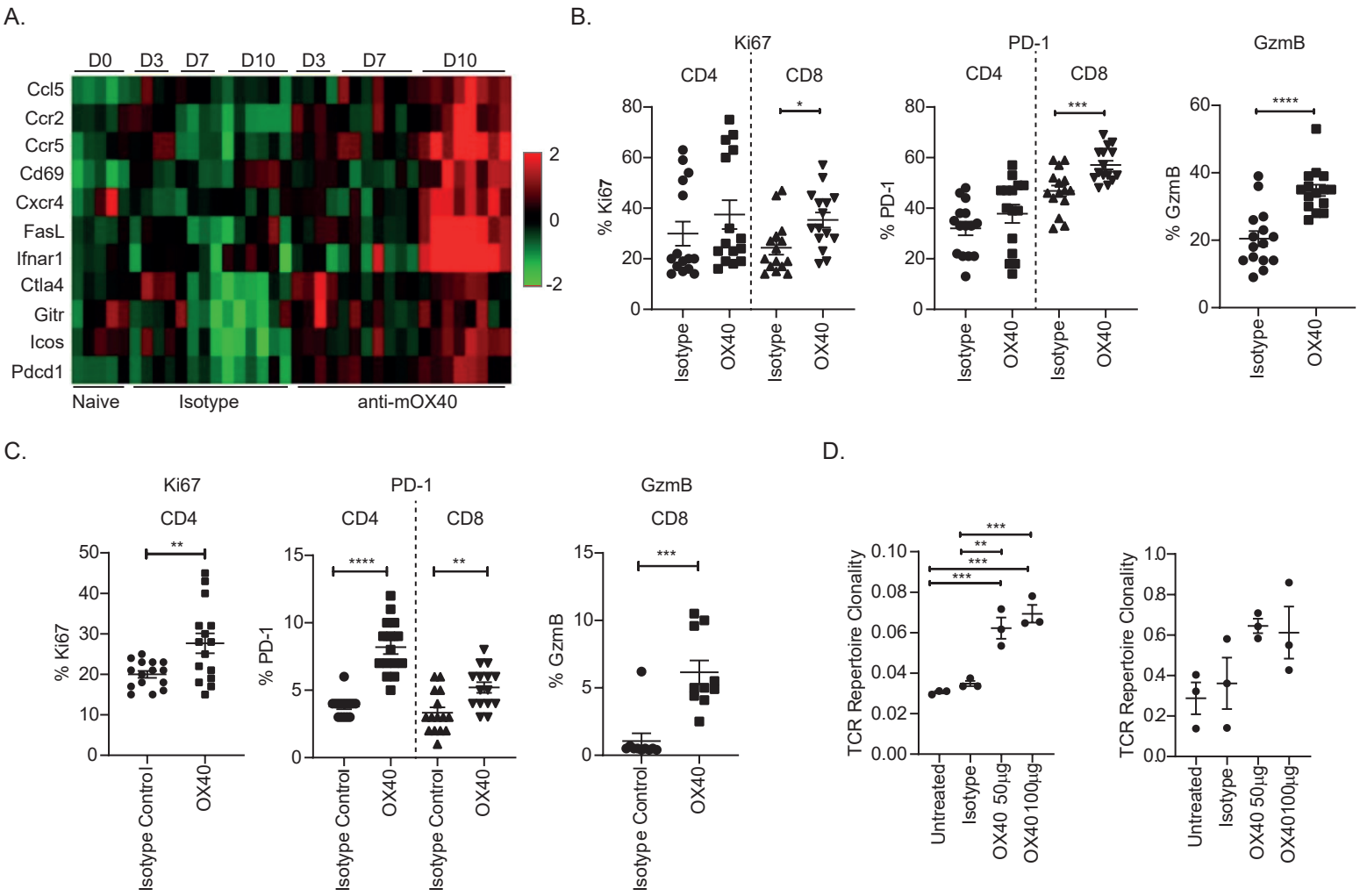

Supplemental Fig. 2. A. Gene expression analysis of CD8+ T cells isolated from A20 tumor-bearing mice treated with 100 μg isotype control or anti-OX40 twice weekly. Mice treated as in schematic shown in Supplemental Fig. 1A. Tumor infiltrate (B) and Blood (C) taken from A20 tumor-bearing mice on Day 10 post randomisation and treated with isotype control or anti-OX40 (200 μg) and analysed for Ki67 (left panel), PD-1 (middle panel) and GzmB (right panel). B. n = 15, pooled from 3 independent experiments C. n = 15 for Ki67 and PD-1, pooled from 3 independent experiments, n = 10 for GzmB, pooled from 2 independent experiments. D. Mice were challenged with $5x10^4$ CT26 tumor cells and treated with indicated doses of anti-OX40. Spleens (left panel) and tumor (right panel) were harvested 7 days post assignment to treatment groups and assessed for TCR repertoire clonality n=3, one experiment. **** $p < 0.0001$, *** $p<0.001$, ** $p < 0.01$, * $p < 0.05$ Mean +/- SEM B & C – unpaired T-Test, D - Tukey's mutliple comparison one-way ANOVA

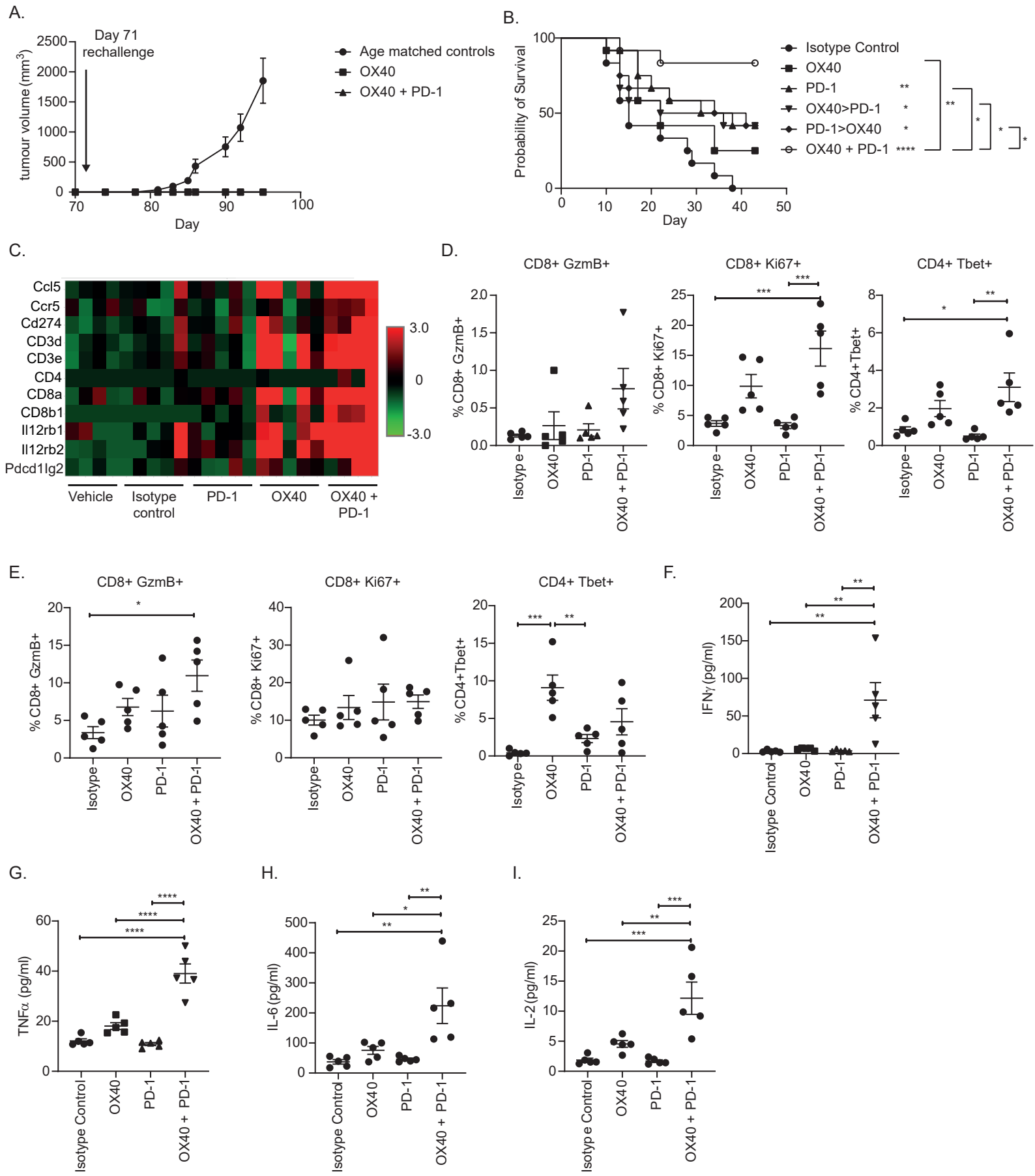

Supplemental Fig 3. Combination treatment with anti-OX40 and anti-PD-1 leads to increase in Th1 cytokines in CT26 tumor model A.Growth curves of naive mice or long term survivors from set up as in Fig 1F. Mice challenged with CT26 cells ($5x10^4$) on Day 71 n=10 age-matched controls, n=2 OX40 monotherapy and n=14 OX40 + PD-1, one experiment. B. Survival curves of mice challenged with CT26 ($5x10^4$) and treated with 6 doses of Isotype combination (rIgG1 100 μg + rIgG2a 200 μg), OX40 (100 μg), PD-1 (200 μg) or combination given concurrently (OX40+PD-1) or sequentially either as OX40 first (OX40>PD-1) or PD-1 first (PD-1>OX40) n=12, one experiment. C Gene expression analysis of CD8+ TILs harvested on Day 7 n= 4 for vehicle and OX40+PD-1, n=5 for isotype, OX40 and PD-1 monotherapies. D & E. Blood (D) and tumour (E) samples taken on Day 10 immunophenotyped for CD8+GzmB+ (left panels), CD8+Ki67+ (middle panels) and CD4+Tbet+ (right panels). n=5, one experiment. F-I. Serum from mice challenged as in Fig. 1F were analysed for IFNγ (F), TNFα (G), IL-6 (H) and IL-2 (I). n=5 one experiment. **** $p < 0.0001$, *** $p < 0.001$, ** $p < 0.01$, * $p < 0.05$ Mean +/- SEM B - Log rank test, D-I Tukeys one-way ANOVA with multiple comparison.

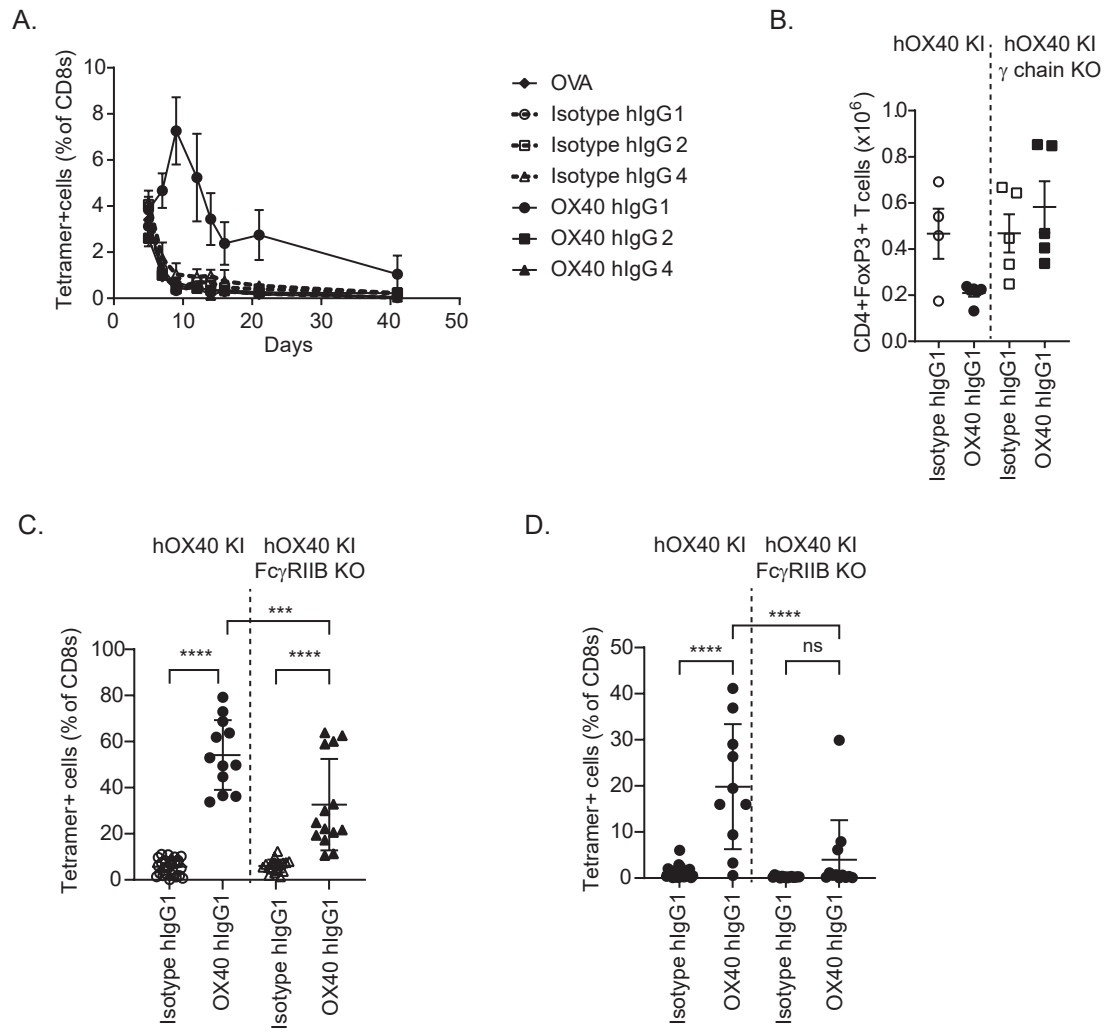

Supplemental Fig 4. anti-OX40 hIgG1 expands OT-I T cells in WT recipients. A. $1x10^5$ hOX40KI$^{+/-}$ OT-I were transferred into WT C57BL/6 recipients and challenged with 5 mg Ova + 100 μg isotype or anti-OX40 mAb. Blood samples were analysed on the indicated days, n=3 representative of 2 independent experiments. B. Splenic analysis of CD4+Foxp3+ T cell numbers on Day 4 post Ova (5 mg) and antibody (100 μg) challenge. Isotype hIgG1 mAb n=4, anti-OX40 hIgG1 mAb n=6, γ chain KO Isotype hIgG1 mAb and anti-OX40 hIgG1 mAb n=5 representative of 2 independent experiments. C. Blood analysis of OT-I T cells on Day 7, Isotype hIgG1 mAb n=16, anti-OX40 hIgG1 mAb n=12 (4 mice excluded due to lack of response), FcγRIIB KO Isotype hIgG1 mAb n=19, FcγRIIB KO anti-OX40 hIgG1 mAb n= 15 (4 mice excluded due to lack of response). Data pooled from 4 independent experiments. D. Blood analysis of OT-I T cells on Day 61, Isotype hIgG1 mAb n=12, anti-OX40 hIgG1 mAb n=10 (2 mice excluded due to a lack of response), FcγRIIB KO Isotype hIgG1 mAb n=15 and anti-OX40 hIgG1 mAb n= 13 (2 mice excluded due to lack of response). Data pooled from 3 independent experiments. **** $p<0.0001$, *** $p<0.01$, Mean +/- sem C & D – Tukey's multiple comparison one way ANOVA

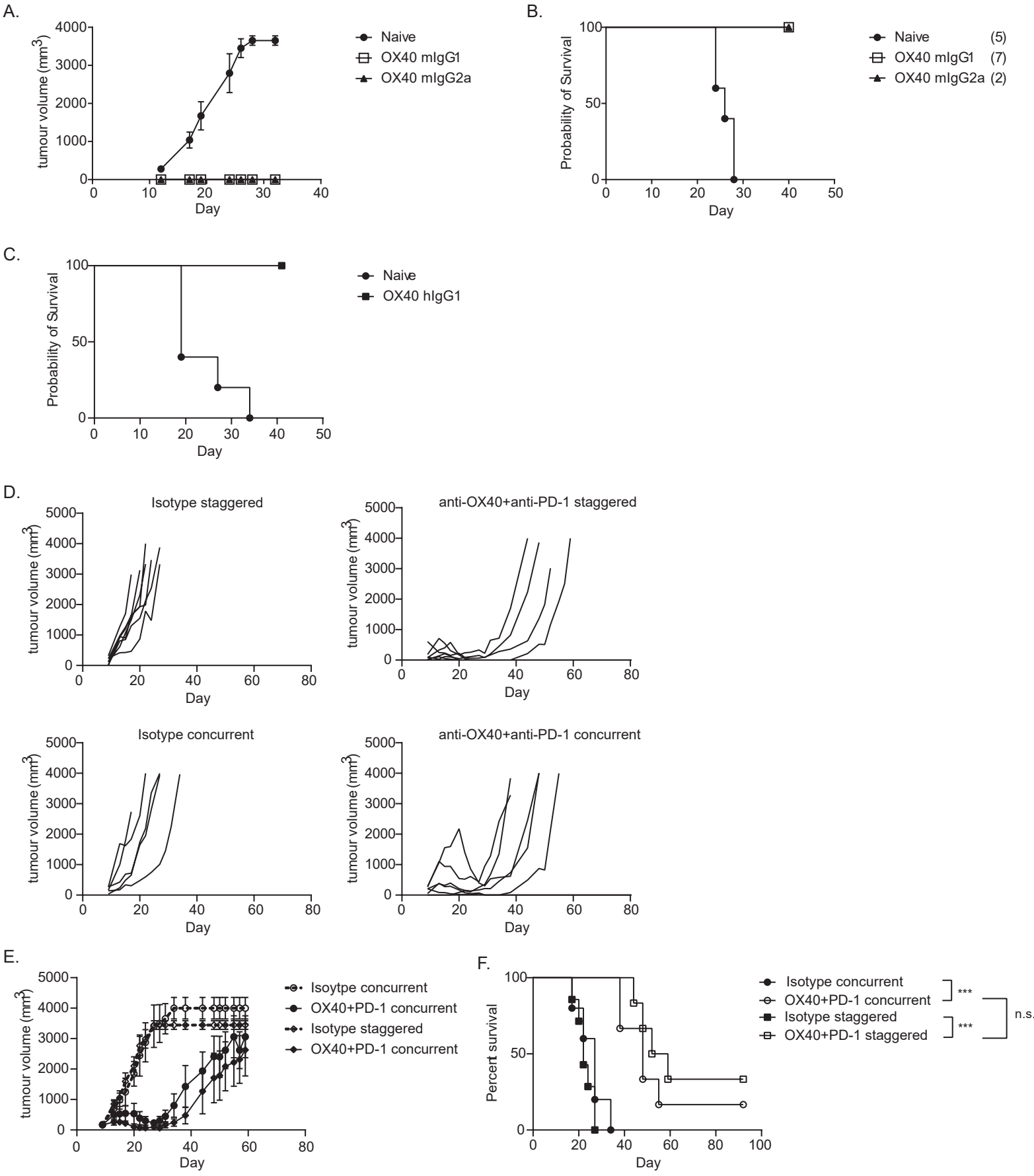

Supplemental Fig 5. Anti-OX40 mAb induces protective memory and is augmented with staggered or concurrent treatment with anti-PD-1 mAb. EG.7 Ova rechallenge experiments with mice previously challenged with EG.7 Ova and treated with anti-OX40 mIgG1 and mIgG2a (A & B) and anti-OX40 hIgG1 (C). Mice were re-challenged with $0.5x10^6$ EG.7 Ova, as were Naive mice to act as controls. Naive mice, n=5, mIgG1 n=7 (A & B), mIgG2a n=2 (A & B), hIgG1 n= 2. D-F Mice challenegd with $0.5x10^6$ EG.7 Ova were treated with anti-OX40 hIgG1 and anti-PD-1 mAb either concurrently or with a staggered dosing schedule. Individual growth curves are shown in (D), combined growth curves in (E) and Survival curves are shown in (F). Isotype concurrent n=5, Isotype staggered n=7, OX40+PD1 concurrent n=6 and OX40+PD-1 staggered n=6 *** $p<0.001$, F - Log rank test.

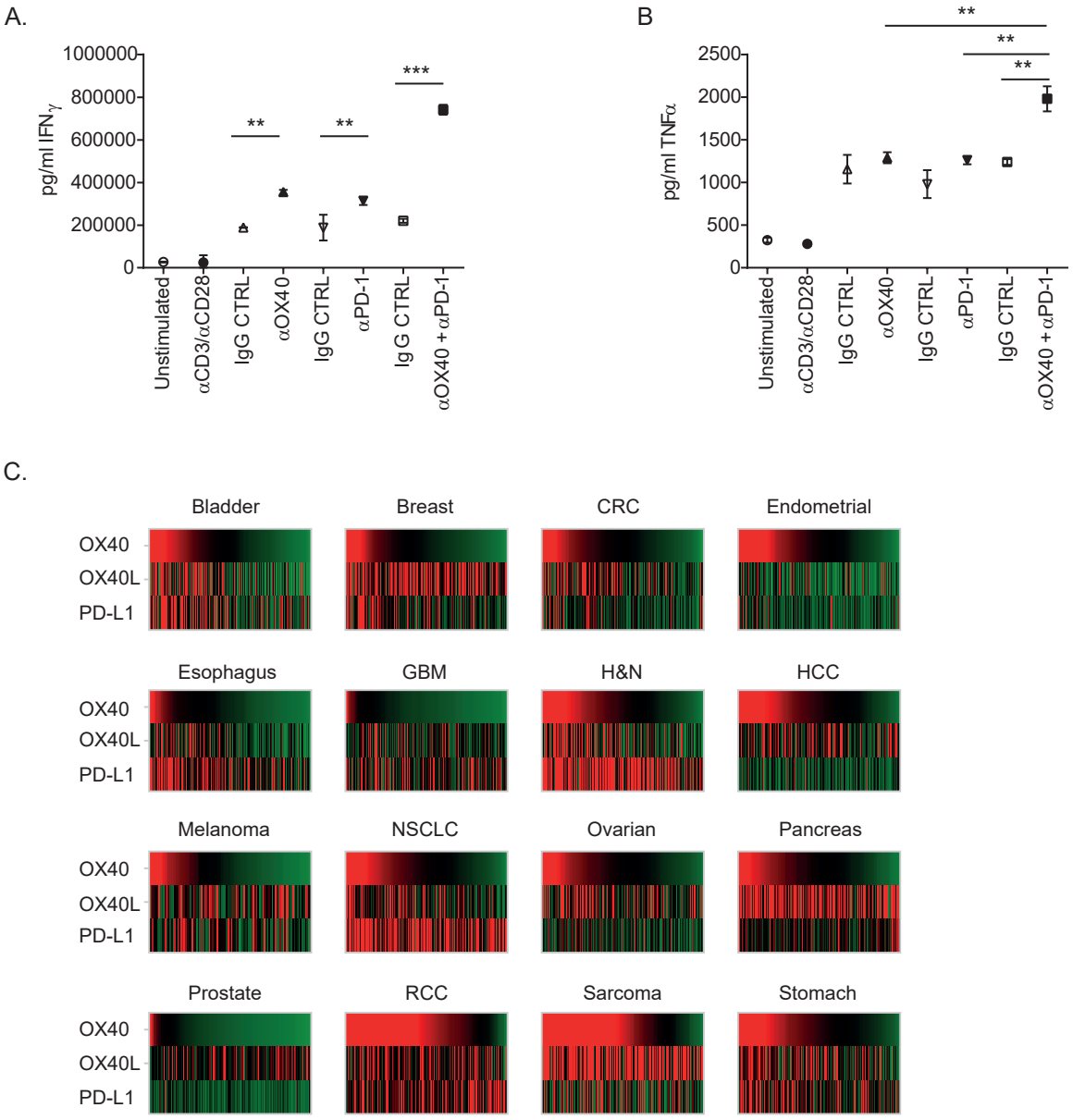

Supplemental Fig 6. OX40 and PD-1 boost Th1 cytokines in PBMCs from healthy donors. A & B. Treatment of healthy hPBMCs cultured in presence of anti-CD3/anti-CD28 expander beads (1:20 ratio) for 48 hours, then restimulated with anti-OX40, pembrolizumab or both (10μg/ml) in the presence of anti-CD3 beads at a 1:1 ratio for a further 4 days. Supernatants tested for IFNγ (A) and TNFα (B). Representative data shown from one of 5 donors. C. OX40, OX40L and PD-L1 abundance in various tumours (stage IV) using RNA-Seq data from TCGA. Expression is based on reads per Kb per million (RPKM). Mean +/- S.E.M. *** p<0.0003, ** p<0.005 A & B - Unpaired t test.